Renewable and Sustainable Energy Reviews 187 (2023) 113698

Contents lists available at ScienceDirect

Renewable and Sustainable Energy Reviews

journal homepage: www.elsevier.com/locate/rser

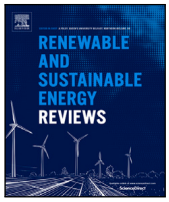

Original research article

Along-wind and cross-wind coupled nonlinear oscillations of wind turbine towers close to 1:1 internal resonance

Stefano Lenci

Department of Civil and Building Engineering and Architecture (DICEA), Polytechnic University of Marche (UNIVPM), via Brecce Bianche, 60131, Ancona, Italy

ARTICLE INFO

Keywords:
Nonlinear dynamics
Wind turbine towers
Along-wind oscillation
Cross-wind oscillation
Internal resonance
Coupled nonlinear vibrations

ABSTRACT

An approximate analytical solution is obtained to detect the along-wind and cross-wind coupled oscillations of wind turbine towers, in the neighbourhood of a 1:1 internal resonance. The obtained formulas are general, and they are applied to the NREL 5-MW reference wind turbine. It is shown that the coupled solution is branched (by a pitchfork bifurcation) from the main uncoupled along-wind oscillation. The coupled motion is initially stable, but for increasing excitation amplitudes it becomes unstable in favour of quasi-periodic solutions, a fact that is particularly dangerous from a practical point of view and so must be avoided. The critical threshold is determined for varying excitation amplitude, and the analytical solution is checked by means of numerical simulations.

1. Introduction

One of the challenges for current and future generations is to reduce the carbon footprint and to achieve climate neutrality. This has been realized by major international institutions (e.g. the European Green New Deal [1]) and requires the production of energy from renewable fonts. Wind [2,3] seems to be the most productive green source when compared with hydropower, solar, biomass, geothermal, etc., see for example [4].

In the field of wind turbines engineering a lot of attention has been devoted to the fluid(flow)-structure interactions [5], since this is a very complex problem, not yet fully understood. Studies have been done by considering blades only [6] or the full machine [7], and mainly dealing with refined numerical methods [8], sometimes also providing comparisons with experimental results [9].

Another promising field of research is FOWTs, which are one of the future directions since the onshore fields for wind turbines are almost totally exploited. The combined presence of aerodynamic [10], structural, hydrodynamics and mooring problems (and control, indeed) poses challenges for modelling [11] and understanding their behaviour [12], and asks for comprehensive theoretical, numerical and experimental [13] analyses.

Despite the large interest recently dedicated to those aspects, structural problems still deserve adequate attention and deep investigation [14]. Many aspects have been addressed, from life cycle assessment [15] to long-term extreme load predictions [16] to load due to waves in offshore turbines [17] to erection and maintenance [18] to vibration [19] and performance [20] control to structural health monitoring [21], just to name few.

In addition to static buckling [22], that however seems to be quite well understood, at least from a theoretical point of view, it is in the realm of dynamical analysis that the major problems arise [23], since excessive vibrations lead to fatigue issues [24].

Dagli et al. [25] studied the dynamics of an offshore wind turbine tower using a numerical analysis considering wind, wave and earthquake forces. Hu et al. [26] performed an important experimental campaign of tall offshore monopile steel wind turbine towers under wind, wave and current during the erection stage. Comparison with numerical results is also reported. Quilligan et al. [27] developed a dynamical model aimed at obtained the fragility curves, i.e. the probability of reaching a limit state as a function of the wind speed. They compared steel and concrete towers, and considered two different heights.

Wang et al. [28] considered a mixed flexible–rigid multi-body model to predict the dynamic performance of a wind turbine system, focusing on the thin-walled beam theory for the tower and the rotor. Harte et al. [29] investigated the along-wind forced vibration response of an onshore wind turbine including the effect of the soil–structure interaction. A very interesting review of structural problems arising in wind turbine towers, including dynamical ones, is reported in [30], while several aspects of dynamic analysis and design have been discussed in [31].

All previous works, and many others indeed, are based on linear analyses (at least for the structural components), so assuming that the displacements are small and the material is linearly elastic, and thus possibly missing important phenomena due to the nonlinearity at the structural level.

E-mail address: lenci@univpm.it.

https://doi.org/10.1016/j.rser.2023.113698
Received 11 March 2023; Received in revised form 20 July 2023; Accepted 29 August 2023

Nomenclature

Abbreviations (listed in alphabetic order)

CM	Centre of mass
dof	Degrees of freedom
FEM	Finite elements method
FOWT	Floating offshore wind turbine
FRC	Frequency response curve
MTSM	Multiple times scale method
MW	Mega watt
NREL	National renewable energy laboratory
NS	Neimark–Sacker
ODE	Ordinary differential equation
SN	Saddle–node
PF	Pitchfork

Notations/Symbols (listed in order of appearance)

x	along-wind horizontal direction
y	cross-wind horizontal direction
z	vertical axis
t	time
$\bar{x}(t)$	displacement along x
$\bar{y}(t)$	displacement along y
$\alpha(t)$	rotation around z (yaw rotation)
$x_{CM}(t)$	displacement along x of CM
$y_{CM}(t)$	displacement along y of CM
d	distance between tower and CM
E_{kin}	kinetic energy
M	mass of the system
$\bar{I}_p$	mass moment of inertia
E_{el}	elastic energy
$\bar{K}_\alpha$	linear stiffness for rotation
$\bar{K}$	linear stiffness for translation
$\bar{K}_3$	nonlinear stiffness for translation
δ	magnitude of the horizontal displacement
$\bar{f}(t)$	force acting on the system
W	work done by the force $\bar{f}(t)$
L	Lagrangian function
$\bar{C}_{x,y,\alpha}$	damping coefficient along x, y and α
I_p	dimensionless moment of inertia
ω_x	natural frequency along x
k_α	dimensionless linear stiffness for rotation
k_3	dimensionless nonlinear stiffness for translation
$c_{x,y,\alpha}$	dimensionless damping coefficient along x, y and α
$x(\tau)$	dimensionless displacement along x
$y(\tau)$	dimensionless displacement along y
τ	dimensionless time
$f(\tau)$	dimensionless force acting on the system
Q	force on top of the wind tower
$\bar{s}(z)$	horizontal displacement of the tower
θ	rotation of the tower
EI_a	bending stiffness of the tower
H	height of the tower
GI_t	torsional stiffness of the tower
G	shear modulus
E	Young modulus
ν	Poisson coefficient
$\omega_{1,2,3}$	dimensionless natural frequencies
ε	small bookkeeping parameter
$x_{1,2,3}$	asymptotic expansions of $x(\tau)$
$y_{1,2,3}$	asymptotic expansions of $y(\tau)$
$\alpha_{1,2,3}$	asymptotic expansions of $\alpha(\tau)$
T_0	fast time
$T_{1,2,...}$	slow times
$cc_{x,y,\alpha}$	rescaled version of $c_{x,y,\alpha}$
F	amplitude of the harmonic excitation
ω	(circular) frequency of the harmonic excitation
I	imaginary unit
σ_e	external detuning parameter
σ_i	internal detuning parameter
$A_x(T_2)$	complex amplitude of the first order oscillation along x
$\bar{A}_x(T_2)$	complex conjugate of $A_x(T_2)$
$A_y(T_2)$	complex amplitude of the first order oscillation along y
$\bar{A}_y(T_2)$	complex conjugate of $A_y(T_2)$
$a_x(T_2)$	real amplitude of the first order oscillation along x
$\phi_x(T_2)$	phase of the first order oscillation along x
$a_y(T_2)$	real amplitude of the first order oscillation along y
$\phi_y(T_2)$	phase of the first order oscillation along y
a_{x0}	amplitude of the periodic oscillation along x
ϕ_{x0}	phase of the periodic oscillation along x
a_{y0}	amplitude of the periodic oscillation along y
ϕ_{y0}	phase of the periodic oscillation along y
f	auxiliar parameter used in (65)
$\hat{G}$	gradient matrix of the modulation equations
λ_i	eigenvalues of $\hat{G}$
$a_{x0,cr}$	critical value of a_{x0} for peak of the FRC
$\sigma_{e,cr}$	critical value of σ_e for peak of the FRC

Parameters not listed above are directly reported in Appendix.

The nonlinear dynamics of a wind turbine tower due to the material, i.e. plasticity, which is needed for investigating collapses [32] and ultimate limit state analysis, has been considered in [33] by a rigid-plastic model.

This research is interested in the serviceability limit state, so that the system works in the linear elastic regime. However, geometrical nonlinearity is considered, since the new wind turbines are very slender and prone to nonlinear effects, that have not yet adequately been investigated.

The nonlinear dynamics of blades have been studied in [34] by numerical models applied to the geometrically exact beam theory. Dai et al. [35] addressed the same problem, but with a focus on fluctuating wind loads and by using a Galerkin approximation. Geometric nonlinearities of the blades are also considered in [36]. In [37] the blades are parked (i.e. they do not rotate) and a continuum model is used.

Sapountzaki et al. [38] used a geometrically nonlinear dynamical model for the wind tower and considered columns of variable cross-section founded either on the surface or on a monopile foundation system subjected to wind and seismic excitations. This work seems to be one of the few that considered the nonlinear behaviour of the pile.

As it is well known [39], geometric nonlinearities in structural components may lead to many phenomena and behaviours missed in

the linear realm, that are potentially dangerous if not properly taken into account or, on the contrary, that are beneficial if adequately exploited. Among many others (e.g. chaos, multistability, etc.), in this work the *internal resonance* is investigated, where the closeness of two natural frequencies causes nonlinear mode coupling, while the modes remain uncoupled in the linear regime.

The 1:2 internal resonance of wind turbine blades has been studied in [40] by using a Galerkin modal reduction and finally considering a 2 dof system; only numerical simulations are reported. Different types of internal resonance, including combination one, have been analysed in [41] using a 4 dof Galerkin model, considering also analytical solutions obtained by the MTSM.

To the best of the author's knowledge, internal resonance of the wind turbine tower has not been previously investigated, even though the symmetrical cross-section automatically induces two natural frequencies that are very close between each other and thus a 1:1 internal resonance naturally arises. It is then expected that along-wind and cross-wind oscillations, that are decoupled in the linear regime, interact in the nonlinear range, which is an unwanted phenomenon since it induces strong vibrations that negatively affect the fatigue life of the tower. For a general treatment of the 1:1 internal resonance the paper [42] is referred to.

The novelty and the main contribution of this work is that it investigates for the first time (to the best of the author's knowledge) the 1:1 internal resonance of wind towers. Thus, it is aimed to fill the previously highlighted gap of knowledge, and is particularly relevant for industry, which has to take this phenomenon into account for a safe and sustainable design, with a reliable lifetime prediction, and for the policymakers, that have to include it in future codes for design.

This work is organized as follows. In Section 2 a simplified, but accurate, nonlinear model of the wind turbine tower is obtained, and the main hypotheses upon which this study is based on are illustrated. The occurrence of 1:1 internal resonance is highlighted in Section 3, and then it is investigated analytically in Section 4. The obtained formulas are very general, and in Section 5 they are illustrated with the NREL 5-MW reference wind turbine [43], including comparison with numerical simulations. Section 6 summarizes the main results and ends the work.

2. The mechanical model and governing equations

The dynamics of the wind turbine tower illustrated in Fig. 1 are studied. It is assumed that the tower is axially rigid so that the nacelle can only translate horizontally, along-wind in the x direction and across-wind in the y direction (see Fig. 1a). The nacelle is connected to the top of the tower, and can rotate around the vertical axis z (yaw rotation). The rotations around the x and y axes are neglected. It is assumed that the wind force is always along the x-axis: this is reasonable because the yaw is assumed to be small. Furthermore, the wind force acts on the CM, whose horizontal coordinates are (see Fig. 1b):

$$x_{CM}(t) = \bar{x}(t) + d\cos(\alpha(t)),$$
$$y_{CM}(t) = \bar{y}(t) + d\sin(\alpha(t)), \tag{1}$$

where d is the horizontal distance between the vertical axis of the tower and CM, $\alpha(t)$ the yaw rotation around the vertical axis z, positive if anticlockwise, $\bar{x}(t)$ and $\bar{y}(t)$ the horizontal displacements of the top of the tower (Fig. 1b).

With the above assumptions, the kinetic energy is given by

$$E_{kin} = \frac{M}{2}(\dot{x}_{CM}^2 + \dot{y}_{CM}^2) + \frac{\bar{I}_p}{2}\dot{\alpha}^2, \tag{2}$$

where M is the modal mass of the (first) vibration mode of the tower–nacelle–rotor blades system (see Section 2.1 for more details), $\bar{I}_p$ the mass moment of inertia with respect to the vertical axis passing through the axis of the tower, and dot means derivative with respect to the physical time t. The considered model has the three mechanical dof $\bar{x}(t)$, $\bar{y}(t)$ and $\alpha(t)$.

The elastic energy is given by

$$E_{el} = \frac{\bar{K}_\alpha}{2}\alpha^2 + \frac{\bar{K}}{2}\delta^2 + \frac{\bar{K}_3}{4}\delta^4 + \dots, \tag{3}$$

where $\delta = \sqrt{\bar{x}^2 + \bar{y}^2}$ is the total displacement of the top of the tower (Fig. 1b). Terms higher than δ^4 are neglected because only moderately large displacements are investigated, and a third order approximation is enough. Since it is assumed that α is small, only the *linear* stiffness $\bar{K}_\alpha$ in rotation is considered. $\bar{K}$ and $\bar{K}_3$ are the linear and nonlinear stiffness of the displacements, and can be computed as shown in Section 2.1.

The work done by the force $\bar{f}(t)$ due to the wind (or by other actions, e.g. the oscillation of the buoy in floating offshore wind turbine) is given by

$$W = \bar{f}(t)x_{CM}(t). \tag{4}$$

From the stationarity of the Lagrangian function $L = E_{kin} - E_{el} + W$ it is possible to obtain the three equations of motions

$$M\ddot{\bar{x}} + \bar{C}_x\dot{\bar{x}} - Md[\dot{\alpha}^2\cos(\alpha) + \ddot{\alpha}\sin(\alpha)] + \bar{K}\bar{x} + \bar{K}_3\bar{x}(\bar{x}^2 + \bar{y}^2) = \bar{f}(t), \tag{5}$$
$$M\ddot{\bar{y}} + \bar{C}_y\dot{\bar{y}} - Md[\dot{\alpha}^2\sin(\alpha) - \ddot{\alpha}\cos(\alpha)] + \bar{K}\bar{y} + \bar{K}_3\bar{y}(\bar{x}^2 + \bar{y}^2) = 0, \tag{6}$$
$$(Md^2 + \bar{I}_p)\ddot{\alpha} + \bar{C}_\alpha\dot{\alpha} - Md[\ddot{\bar{x}}\sin(\alpha) - \ddot{\bar{y}}\cos(\alpha)] + \bar{K}_\alpha\alpha = -\bar{f}(t)d\sin(\alpha), \tag{7}$$

where the damping, which is assumed to be linear in all degrees of freedom, is added. $\bar{C}_x$, $\bar{C}_y$ and $\bar{C}_\alpha$ are the damping coefficients.

It is worth noting that there are nonlinearities in the inertia and in the (translational) stiffnesses. Along y there is no excitation (see (6)), according to the previous hypothesis on the wind direction. The torsional–translational behaviour has been studied in [44], but focusing only on the tower and in the linear regime, using FEM and assuming earthquake excitations.

Since the goal is an analytical treatment of the problem, it is convenient to work with dimensionless quantities. Introducing the following dimensionless parameters and variables

$$I_p = \frac{\bar{I}_p}{Md^2}, \quad \omega_x = \sqrt{\frac{\bar{K}}{M}}, \quad k_\alpha = \frac{\bar{K}_\alpha}{\bar{K}d^2}, \quad k_3 = \frac{\bar{K}_3 d^2}{\bar{K}},$$
$$c_x = \frac{\bar{C}_x}{2\omega_x M}, \quad c_y = \frac{\bar{C}_y}{2\omega_x M}, \quad c_\alpha = \frac{\bar{C}_\alpha}{2\omega_x Md^2},$$
$$x(\tau) = \frac{\bar{x}(t)}{d}, \quad y(\tau) = \frac{\bar{y}(t)}{d}, \quad \tau = \omega_x t, \quad f(\tau) = \frac{\bar{f}(t)}{\bar{K}d}, \tag{8}$$

the Eqs. (5)–(7) become

$$\ddot{x} + 2c_x\dot{x} - [\dot{\alpha}^2\cos(\alpha) + \ddot{\alpha}\sin(\alpha)] + x + k_3x(x^2 + y^2) = f(\tau), \tag{9}$$
$$\ddot{y} + 2c_y\dot{y} - [\dot{\alpha}^2\sin(\alpha) - \ddot{\alpha}\cos(\alpha)] + y + k_3y(x^2 + y^2) = 0, \tag{10}$$
$$(1 + I_p)\ddot{\alpha} + 2c_\alpha\dot{\alpha} - [\ddot{x}\sin(\alpha) - \ddot{y}\cos(\alpha)] + k_\alpha\alpha = -f(\tau)\sin(\alpha), \tag{11}$$

where now dot means derivative with respect to the dimensionless time τ. Note that ω_x is the physical natural (linear) circular frequency in the x direction, that is decoupled from y and α in the linear regime (see forthcoming Section 3). The parameters are I_p, k_α, k_3 and the damping coefficients c_x, c_y and c_α.

To obtain the numerical solutions of forthcoming Section 5.1 it is needed to rearrange the previous equations to have only one second order derivative on the left hand side of each equation:

$$\begin{aligned}\ddot{x} &= -x(x^2 + y^2)k_3 + \dot{\alpha}^2\cos(\alpha) - 2c_x\dot{x} - x + f(\tau)\\ &+ \frac{1}{I_p}[(-\sin(\alpha)x + \cos(\alpha)y)\sin(\alpha)(x^2 + y^2)k_3\\ &(-\sin(\alpha)x + \cos(\alpha)y)\sin(\alpha) - \sin(\alpha)\alpha k_\alpha\\ &- 2c_x\dot{x}\sin(\alpha)^2 + 2c_y\dot{y}\sin(\alpha)\cos(\alpha) - 2c_\alpha\dot{\alpha}\sin(\alpha)],\\ \ddot{y} &= -y(x^2 + y^2)k_3 + \dot{\alpha}^2\sin(\alpha) - 2c_y\dot{y} - y\\ &+ \frac{1}{I_p}[(-\cos(\alpha)y + \sin(\alpha)x)\cos(\alpha)(x^2 + y^2)k_3\end{aligned} \tag{12}$$

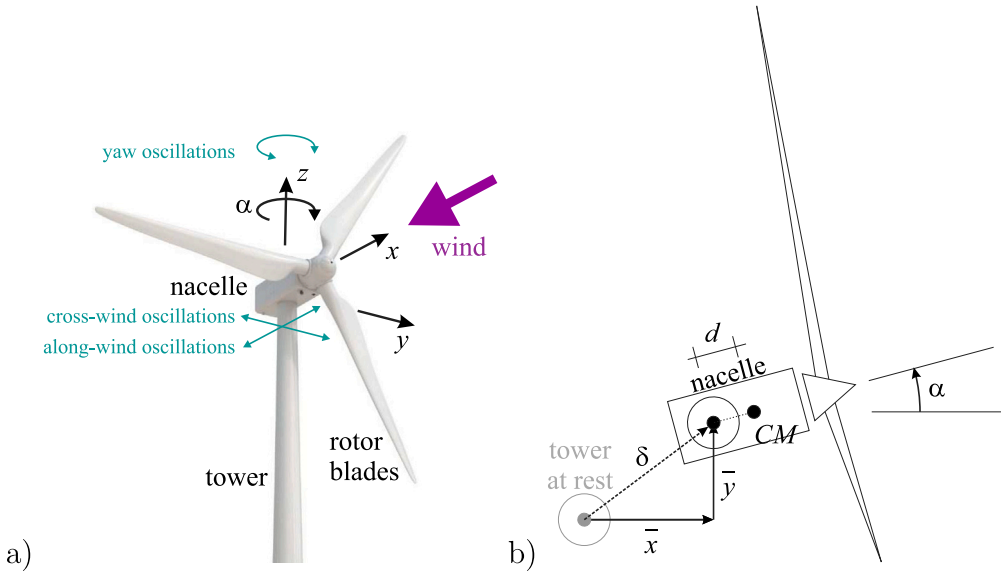

Fig. 1. (a) The mechanical model and (b) top view, schematic and coordinates.

$$(-\cos(\alpha)y+\sin(\alpha)x)\cos(\alpha)+\cos(\alpha)\alpha k_\alpha$$
$$-\,2c_y\dot{y}\cos(\alpha)^2+2c_x\dot{x}\sin(\alpha)\cos(\alpha)+2c_\alpha\dot{\alpha}\cos(\alpha)], \tag{13}$$

$$\ddot{\alpha}=\frac{1}{I_p}[(\cos(\alpha)y-\sin(\alpha)x)(x^2+y^2)k_3$$
$$+\,\cos(\alpha)y-\sin(\alpha)x-k_\alpha\alpha$$
$$+\,2c_y\dot{y}\cos(\alpha)-2c_x\dot{x}\sin(\alpha)-2c_\alpha\dot{\alpha}]. \tag{14}$$

2.1. The translational and rotational stiffnesses

To compute the stiffnesses $\bar{K}$ and $\bar{K}_3$, the wind turbine tower is considered as a cantilevered vertical beam with an horizontal force Q on the top; because of the axial symmetry it is possible to consider a planar problem, with transversal displacement denoted $\bar{s}(z)$.

Neglecting the axial and the shear deformations, the beam can be considered as an "elastica" [45], which is governed by the equations

$$\bar{s}'=\sin\theta,$$
$$EI_a\theta''+Q\cos\theta=0, \tag{15}$$

where prime denotes derivative with respect to spatial vertical coordinate z, θ is the deflection angle and EI_a the bending stiffness of the beam. The boundary conditions are $\bar{s}(0)=0$ and $\theta(0)=0$ (fixed bottom). Although a closed form solution of (15) is available, for the scope of the this work an asymptotic expansion is enough. The computations give

$$Q=\frac{EI_a}{H^2}\left[3\frac{\delta}{H}+\frac{108}{35}\left(\frac{\delta}{H}\right)^3+\frac{48357}{13475}\left(\frac{\delta}{H}\right)^5+\cdots\right], \tag{16}$$

where $\delta=\bar{s}(H)$ is the top displacement, so that the elastic energy is

$$E_{el}=\frac{1}{2}\frac{3EI_a}{H^3}\delta^2+\frac{1}{4}\frac{108}{35}\frac{EI_a}{H^5}\delta^4+\frac{1}{6}\frac{48357}{13475}\frac{EI_a}{H^7}\delta^6+\ldots. \tag{17}$$

By comparing (3) with (17) it is immediate to conclude that

$$\bar{K}=\frac{3EI_a}{H^3},\quad \bar{K}_3=\frac{108}{35}\frac{EI_a}{H^5}. \tag{18}$$

It follows that

$$k_3=\frac{\bar{K}_3d^2}{\bar{K}}=\frac{36}{35}\left(\frac{d}{H}\right)^2,\quad f(\tau)=\bar{f}(t)\frac{H^2}{3EI_a}\frac{H}{d}, \tag{19}$$

The tower is considered as a cantilever also with respect to its torsional behaviour, but now within a linear realm since the tower is much more rigid in torsion than in bending, because of its tubular cross-section. It follows

$$\bar{K}_\alpha=\frac{GI_t}{H}, \tag{20}$$

where GI_t is the torsional stiffness, so that

$$k_\alpha=\frac{\bar{K}_\alpha}{\bar{K}d^2}=\frac{GI_t}{EI_a}\left(\frac{H}{d}\right)^2. \tag{21}$$

For cross-sections with a polar symmetry $I_t=2I_a$. If the material is isotropic $G=E/(2+2\nu)$ (E being the Young modulus and ν the Poisson coefficient), and thus

$$k_\alpha=\frac{1}{(1+\nu)}\left(\frac{H}{d}\right)^2. \tag{22}$$

Since in real applications $d<<H$, it follows that k_α is a large dimensionless number.

In above developments there are two main assumptions:

- the cross-section of the tower is constant. This represents a good approximation of the real case, certainly catching the order of magnitude of the stiffness, by considering the average cross-section. For a more detailed analysis of a non-constant cross-section [46] is refer to;
- the junction between the tower and the nacelle is perfect. In practice there is a stiffness also in the joint, likely related to the yaw control systems, which however can be easily taken into account in the proposed formulation, and often are negligible with respect to the considered one when the tower is very slender.

3. The natural frequencies

To compute the natural frequencies of the proposed model, the linear unforced undamped version of (9)–(11) is considered:

$$\ddot{x}+x=0, \tag{23}$$
$$\ddot{y}+\ddot{\alpha}+y=0, \tag{24}$$
$$(1+I_p)\ddot{\alpha}+\ddot{y}+k_\alpha\alpha=0. \tag{25}$$

It is observed that in the linear regime the along-wind displacement x is independent of the cross-wind displacement y and rotation α, which instead are coupled between each other.

The three natural frequencies are

$$\omega_1=1, \tag{26}$$

$$\omega_{2,3} = \sqrt{\frac{1 + I_p + k_\alpha \mp \sqrt{(1+I_p)^2 + k_\alpha(2 - 2I_p + k_\alpha)}}{2I_p}}. \tag{27}$$

For very large values of the rotational stiffness k_α (see the comment after Eq. (22)) the following asymptotic development holds:

$$\omega_2 = 1 - \frac{1}{2k_\alpha} + \frac{3 - 4I_p}{8k_\alpha^2} + \dots, \tag{28}$$

$$\omega_3 = \frac{\sqrt{k_\alpha}}{\sqrt{I_p}} + \frac{1}{2\sqrt{I_p}\sqrt{k_\alpha}} + \frac{4I_p - 1}{8\sqrt{I_p}k_\alpha^{3/2}} + \dots, \tag{29}$$

so that it is concluded that ω_3 is very large, while $\omega_1 \approx \omega_2$ and a 1:1 internal resonance occurs [42,47], with a detuning $\omega_1 - \omega_2 \approx \frac{1}{2k_\alpha} + \dots$. As it is well known, it entails a coupling and complex behaviour, that requires to take into account the nonlinear terms, which is the goal of the next section.

4. The nonlinear problem

To address the nonlinear problem the MTSM is used [47], up to the third order. Although it provides an approximate solution, that can fail for large excitation amplitudes [48] (this is the main limitation of the proposed analytical solution), it is appealing since it gives analytical expressions that are easy to manage and accurate enough for small and moderate displacements. If there is an interest to study large displacements, the proposed solution must be extended to fifth (or higher) order terms, without any conceptual difficulty but with more computations.

According to the MTSM the solution is sought after in the form

$$\begin{aligned}
x(\tau) &= \varepsilon x_1(T_0, T_2, \dots) + \varepsilon^2 x_2(T_0, T_2, \dots) + \varepsilon^3 x_3(T_0, T_2, \dots) + \\
y(\tau) &= \varepsilon y_1(T_0, T_2, \dots) + \varepsilon^2 y_2(T_0, T_2, \dots) + \varepsilon^3 y_3(T_0, T_2, \dots) + \\
\alpha(\tau) &= \varepsilon \alpha_1(T_0, T_2, \dots) + \varepsilon^2 \alpha_2(T_0, T_2, \dots) + \varepsilon^3 \alpha_3(T_0, T_2, \dots) + ,
\end{aligned} \tag{30}$$

where $T_0 = \tau$ and $T_i = \varepsilon^i \tau$ are the slow times. Note that it has been shown (computations not reported, but standard in the realm of MTSM) that the solution does depend on T_1, and thus this dependence is omitted in (30). Furthermore, it is assumed that the damping is small,

$$c_x = \varepsilon^2 c c_x, \quad c_y = \varepsilon^2 c c_y, \quad c_\alpha = \varepsilon^2 c c_\alpha, \tag{31}$$

and that the external excitation is small and harmonic,

$$f(\tau) = \varepsilon^3 F \cos(\omega T_0) = \varepsilon^3 \frac{F}{2}\left(e^{I\omega T_0} + e^{-I\omega T_0}\right), \tag{32}$$

where ω is the (circular) frequency of the external excitation and I the imaginary unit.

The assumption that the force due to the wind is harmonic is of course very rough, and corresponds to taking only one term in the Fourier series approach used in [27] for the wind force. It can be used for the oscillatory part of the wind, this being supported by the fact that close to the resonance, the most dangerous case which is of interest in this work, the system response is mainly influenced only by a "single" (the resonant one) frequency, among the many contained in the wind force, as the structure somehow acts as a filter. In any case, this hypothesis is enough to illustrate the occurrence of coupled along-wind and cross-wind nonlinear oscillations, which is the main goal of this work.

Although explicit reference is made to wind thrust, the excitation can come also from other sources, like for example earthquake, waves in offshore applications, etc. (see for example [25] or other works quoted in the introduction).

The worst case situation is considered, i.e. when there is a resonance between the natural (internal) and the external frequencies. More precisely, it is assumed that

$$\omega = \omega_1 + \varepsilon^2 \sigma_e = 1 + \varepsilon^2 \sigma_e, \tag{33}$$

where $\sigma_e \approx \omega - \omega_1$ is the *external* detuning parameter, measuring the frequency mismatch.

It is also assumed to be closed to the 1:1 internal resonance, which occurs for k_α very large, as it is in common cases (see Section 3). In particular,

$$1 = \omega_1 = \omega_2 + \varepsilon^2 \sigma_i, \tag{34}$$

where $\sigma_i \approx \omega_1 - \omega_2$ is the *internal* detuning parameter. From (28) it follows $\varepsilon^2 \sigma_i \approx 1/2k_\alpha$.

Based on the previous assumptions, the following relations hold:

$$\begin{aligned}
\omega T_0 &= T_0 + \varepsilon^2 T_0 \sigma_e = T_0 + \sigma_e T_2, \\
\omega T_0 &= (\omega_2 T_0 + \sigma_i T_2) + \sigma_e T_2 = \omega_2 T_0 + (\sigma_i + \sigma_e) T_2, \\
\omega_1 T_0 &= \omega_2 T_0 + \varepsilon^2 T_0 \sigma_i = \omega_2 T_0 + \sigma_i T_2, \\
\omega_2 T_0 &= \omega_1 T_0 - \sigma_i T_2.
\end{aligned} \tag{35}$$

They will be used in the following.

Inserting the previous expressions in (9)–(11), taking into account the chain derivative rule and equating to zero each power of ε, a sequence of successive problems is obtained and discussed in the following subsections.

4.1. First order problem

The first order problem is given by

$$\begin{aligned}
\frac{\partial^2 x_1}{\partial T_0^2} + x_1 &= 0, \\
\frac{\partial^2 y_1}{\partial T_0^2} + \frac{\partial^2 \alpha_1}{\partial T_0^2} + y_1 &= 0, \\
(1 + I_p)\frac{\partial^2 \alpha_1}{\partial T_0^2} + \frac{\partial^2 y_1}{\partial T_0^2} + k_\alpha \alpha_1 &= 0.
\end{aligned} \tag{36}$$

It is exactly the problem (23)–(25), and the solution is given by

$$\begin{aligned}
x_1(T_0, T_2) &= A_x(T_2) e^{\omega_1 I T_0} + \bar{A}_x(T_2) e^{-\omega_1 I T_0}, \\
y_1(T_0, T_2) &= A_y(T_2) e^{\omega_2 I T_0} + \bar{A}_y(T_2) e^{-\omega_2 I T_0}, \\
\alpha_1(T_0, T_2) &= c_1 y_1(T_0, T_2),
\end{aligned} \tag{37}$$

where bar stands for the complex conjugate, $\omega_1 = 1$ (see (26)), ω_2 is given by (27), and c_1 is reported in Appendix. Since $c_1 \approx \omega_1 - \omega_2$, it is small because of the closeness to the 1:1 internal resonance. Thus, the rotation has a much smaller amplitude than the cross-wind translation.

4.2. Second order problem

The second order problem is given by

$$\begin{aligned}
&\frac{\partial^2 x_2}{\partial T_0^2} + x_2 = \alpha_1 \frac{\partial^2 \alpha_1}{\partial T_0^2} + \left(\frac{\partial \alpha_1}{\partial T_0}\right)^2 = \\
&= -\frac{2(\omega_2^2 - 1)^2}{\omega_2^2}\left[A_y^2 e^{2\omega_y I T_0} + \bar{A}_y^2 e^{-2\omega_y I T_0}\right], \\
&\frac{\partial^2 y_2}{\partial T_0^2} + \frac{\partial^2 \alpha_2}{\partial T_0^2} + y_2 = 0, \\
&(1 + I_p)\frac{\partial^2 \alpha_2}{\partial T_0^2} + \frac{\partial^2 y_2}{\partial T_0^2} + k_\alpha \alpha_2 = \alpha_1 \frac{\partial^2 x_1}{\partial T_0^2} = \\
&= \left(-1 + \frac{1}{\omega_y^2}\right)\left[\bar{A}_x \bar{A}_y e^{-I(1+\omega_2)T_0}\right. \\
&\left. + A_x A_y e^{I(1+\omega_2)T_0} + A_x \bar{A}_y e^{I(1-\omega_2)T_0} + \bar{A}_x A_y e^{I(-1+\omega_2)T_0}\right].
\end{aligned} \tag{38}$$

It is noted that there are no secular terms on the right hand sides of (38), i.e. no terms proportional to $e^{\pm I T_0}$ on the right hand side of the first equation and to $e^{\pm I\omega_2 T_0}$ on the right hand side of the second and third equations. This is a consequence of the assumed independence of

T_1, and entails that there is no need to use solvability conditions. The second order solutions are then (the dependence of A_x and A_y on T_2 is omitted to simplify the formulas):

$$
\begin{aligned}
&x_2(T_0,T_2) = c_2\left(A_y^2 e^{2I\omega_2 T_0} + \bar{A}_y^2 e^{-2I\omega_2 T_0}\right),\\
&y_2(T_0,T_2) = c_3\left(A_x A_y e^{I(1+\omega_2)T_0} + \bar{A}_x \bar{A}_y e^{-I(1+\omega_2)T_0}\right)\\
&+\ c_4\left(\bar{A}_x A_y e^{I(-1+\omega_2)T_0} + A_x \bar{A}_y e^{I(1-\omega_2)T_0}\right),\\
&\alpha_2(T_0,T_2) = c_5 c_3\left(A_x A_y e^{I(1+\omega_2)T_0} + \bar{A}_x \bar{A}_y e^{-I(1+\omega_2)T_0}\right)\\
&+\ c_6 c_4\left(\bar{A}_x A_y e^{I(-1+\omega_2)T_0} + A_x \bar{A}_y e^{I(1-\omega_2)T_0}\right),
\end{aligned}
\tag{39}
$$

where $c_2 - c_6$ are reported in Appendix. Note that the singularity of c_6 for $\omega_2 \approx 1 = \omega_1$ is only apparent since in α_2 the constant c_6 is multiplied by c_4 and the denominator simplifies.

4.3. Third order problem

The third order problem is given by

$$
\begin{aligned}
&\frac{\partial^2 x_3}{\partial T_0^2} + x_3 = -k_3 x_1(x_1^2 + y_1^2) - 2cc_x\frac{\partial x_1}{\partial T_0} + \alpha_1\frac{\partial^2 \alpha_2}{\partial T_0^2} + \alpha_2\frac{\partial^2 \alpha_1}{\partial T_0^2}\\
&+\ 2\frac{\partial \alpha_1}{\partial T_0}\frac{\partial \alpha_2}{\partial T_0} - 2\frac{\partial^2 x_1}{\partial T_2 \partial T_0} + \frac{F}{2}\left(e^{I\omega T_0} + e^{-I\omega T_0}\right) = \cdots =\\
&= H_1 e^{3IT_0} + H_2 e^{IT_0} + \bar{H}_1 e^{-3IT_0} + \bar{H}_2 e^{-IT_0},\\
&\frac{\partial^2 y_3}{\partial T_0^2} + \frac{\partial^2 \alpha_3}{\partial T_0^2} + y_3 = -k_3 y_1(x_1^3 + y_1^2) - 2cc_x\frac{\partial y_1}{\partial T_0} + \alpha_1\left(\frac{\partial \alpha_1}{\partial T_0}\right)^2\\
&+\ \frac{\alpha_1^2}{2}\frac{\partial^2 \alpha_1}{\partial T_0^2} - 2\frac{\partial^2 (y_1 + \alpha_1)}{\partial T_2 \partial T_0} = \cdots =\\
&= H_3 e^{3I\omega_2 T_0} + H_4 e^{I\omega_2 T_0} + \bar{H}_3 e^{-3\omega_2 IT_0} + \bar{H}_4 e^{-I\omega_2 T_0},\\
&(1+I_p)\frac{\partial^2 \alpha_3}{\partial T_0^2} + \frac{\partial^2 y_3}{\partial T_0^2} + k_\alpha \alpha_3 = -2cc_\alpha\frac{\partial \alpha_1}{\partial T_0} + \alpha_2\frac{\partial^2 x_1}{\partial T_0^2} + \alpha_1\frac{\partial^2 x_2}{\partial T_0^2}\\
&+\ \frac{\alpha_1^2}{2}\frac{\partial^2 y_1}{\partial T_0^2} - 2\frac{\partial^2 [y_1 + (1+I_p)\alpha_2]}{\partial T_2 \partial T_0} = \cdots =\\
&= H_5 e^{3I\omega_2 T_0} + H_6 e^{I\omega_2 T_0} + \bar{H}_5 e^{-3I\omega_2 T_0} + \bar{H}_6 e^{-I\omega_2 T_0},
\end{aligned}
\tag{40}
$$

where the expressions of $H_1 - H_6$ are reported in Appendix.

Contrarily to the second order problem, now there are secular terms on the right hand side of the previous equations. This requires the solvability conditions, that are given by (the minus is just for convenience, and of course does not affect the results)

$$
\begin{aligned}
&0 = -H_2 = 2I\frac{\partial A_x}{\partial T_2} + 2Icc_x A_x + (c_1 c_4 c_6(2\omega_2 - 1)^2 + k_3)\bar{A}_x A_y^2 e^{-2I\sigma_i T_2}\\
&+\ 3k_3 A_x^2 \bar{A}_x + [c_1(c_3 c_5 + c_4 c_6) + 2k_3]A_x A_y \bar{A}_y - \frac{F}{2}e^{I\sigma_e T_2},
\end{aligned}
\tag{41}
$$

$$
\begin{aligned}
&0 = -H_4 - c_1 H_6 = 2I\omega_2[c_1^2 I_p + (1+c_1)^2]\frac{\partial A_y}{\partial T_2} + 2I\omega_2(cc_y + c_1^2 cc_\alpha)A_y\\
&+\ (c_1 c_4 c_6 + k_3)A_x^2 \bar{A}_y e^{-2I\sigma_i T_2} + [2c_1^2(c_1 + 2c_2)\omega_2^2 + 3k_3]A_y^2 \bar{A}_y\\
&+\ [c_1(c_3 c_5 + c_4 c_6) + 2k_3]A_x \bar{A}_x A_y.
\end{aligned}
\tag{42}
$$

The previous are two complex equations in the two complex unknowns $A_x(T_2)$ and $A_y(T_2)$, by means of which the first order and the second order solutions are obtained through (37) and (39).

4.4. Modulation equations

It is customary [47] to deal with real variables, introducing amplitudes and phases by means of

$$
\begin{aligned}
A_x(T_2) &= \frac{1}{2}a_x(T_2)e^{I[\sigma_e T_2 + \phi_x(T_2)]},\\
A_y(T_2) &= \frac{1}{2}a_y(T_2)e^{I[(\sigma_e + \sigma_i)T_2 + \phi_y(T_2)]},
\end{aligned}
\tag{43}
$$

where now the four *real* unknowns are $a_x(T_2)$, $a_y(T_2)$, $\phi_x(T_2)$ and $\phi_y(T_2)$. Using the expressions (43) the first and second order solutions become (use is made of (35), the dependence on T_2 is omitted to simplify the formulas)

$$
\begin{aligned}
x_1 &= a_x\cos(T_0 + \sigma_e T_2 + \phi_x) = a_x\cos(\omega t + \phi_x),\\
y_1 &= a_y\cos[\omega_2 T_0 + (\sigma_e + \sigma_i)T_2 + \phi_y] = a_y\cos(\omega t + \phi_y),\\
\alpha_1 &= c_1 y_1,\\
x_2 &= \cdots = \frac{a_y^2}{2}c_2\cos(2\omega t + 2\phi_y),\\
y_2 &= \cdots = \frac{a_x a_y}{2}[c_3\cos(2\omega t + \phi_x + \phi_y) + c_4\cos(\phi_x - \phi_y)],\\
\alpha_2 &= \cdots = \frac{a_x a_y}{2}[c_3 c_5\cos(2\omega t + \phi_x + \phi_y) + c_4 c_6\cos(\phi_x - \phi_y)],
\end{aligned}
\tag{44}
$$

that better clarify that $a_x(T_2)$ and $a_y(T_2)$ are amplitudes and $\phi_x(T_2)$ and $\phi_y(T_2)$ phases of the first order harmonic oscillation, and that the second order solution vanishes for $a_y = 0$, i.e. for single mode along-wind oscillation (see Section 4.5).

Inserting (43) in (41)–(42) separating the real and imaginary parts and rearranging, the following four *real* modulation equations are obtained:

$$
\begin{aligned}
&\frac{da_x}{dT_2} = -cc_x a_x + \frac{c_1 c_4 c_6(2\omega_2 - 1)^2 + k_3}{8}\sin[2(\phi_x - \phi_y)]a_x a_y^2\\
&-\ \frac{F}{2}\sin(\phi_x),
\end{aligned}
\tag{45}
$$

$$
\begin{aligned}
&[c_1^2 I_p + (1+c_1)^2]\omega_2\frac{da_y}{dT_2} = -(cc_y + c_1^2 cc_\alpha)\omega_2 a_y\\
&-\ \frac{c_1 c_4 c_6 + k_3}{8}\sin[2(\phi_x - \phi_y)]a_x^2 a_y,
\end{aligned}
\tag{46}
$$

$$
\begin{aligned}
&a_x\frac{d\phi_x}{dT_2} = \frac{3k_3}{8}a_x^3 + \frac{c_1 c_4 c_6(2\omega_2 - 1)^2 + k_3}{8}\cos[2(\phi_x - \phi_y)]a_x a_y^2\\
&+\ \frac{c_1(c_3 c_5 + c_4 c_6) + 2k_3}{8}a_x a_y^2 - \sigma_e a_x - \frac{F}{2}\cos(\phi_x),
\end{aligned}
\tag{47}
$$

$$
\begin{aligned}
&[c_1^2 I_p + (1+c_1)^2]\omega_2 a_y\frac{d\phi_y}{dT_2} = \frac{c_1 c_4 c_6 + k_3}{8}\cos[2(\phi_x - \phi_y)]a_x^2 a_y\\
&+\ \frac{c_1(c_3 c_5 + c_4 c_6) + 2k_3}{8}a_x^2 a_y + \frac{2c_1^2\omega_2^2(c_1 + 2c_2) + 3k_3}{8}a_y^3\\
&-\ [c_1^2 I_p + (1+c_1)^2]\omega_2(\sigma_i + \sigma_e)a_y.
\end{aligned}
\tag{48}
$$

4.5. Single mode along-wind oscillation

Since the excitation is only in the x direction, it is reasonable to foresee that there exists a *single mode* solution involving displacements only along-wind, i.e. a solution with $a_y(T_2) = 0$. In this case (45) and (47) become, respectively,

$$
\begin{aligned}
\frac{da_x}{dT_2} &= -cc_x a_x - \frac{F}{2}\sin(\phi_x),\\
a_x\frac{d\phi_x}{dT_2} &= \frac{3k_3}{8}a_x^3 - \sigma_e a_x - \frac{F}{2}\cos(\phi_x),
\end{aligned}
\tag{49}
$$

which are the classical modulation equations for the Duffing oscillator [47]. Eq. (46) is automatically satisfied. Also (48) is satisfied since all terms are multiplied by a_y. However, eliminating first the common factor a_y, and only after assuming $a_y = 0$, it is obtained

$$
\begin{aligned}
&[c_1^2 I_p + (1+c_1)^2]\omega_2\frac{d\phi_y}{dT_2} = \frac{c_1 c_4 c_6 + k_3}{8}\cos[2(\phi_x - \phi_y)]a_x^2\\
&+\ \frac{c_1(c_3 c_5 + c_4 c_6) + 2k_3}{8}a_x^2 - [c_1^2 I_p + (1+c_1)^2]\omega_2(\sigma_i + \sigma_e),
\end{aligned}
\tag{50}
$$

which is the equation that governs the slow time evolution of $\phi_y(T_2)$. It is needed only from a mathematical point of view, since when $a_y(T_2) = 0$ the behaviour of $\phi_y(T_2)$ is unessential from an engineering point of view, see (44).

Although this is the most intuitive solution, as clearly said in the introduction the main goal of this work is to look for the existence of other, in particular *coupled* along-wind and cross-wind, solutions.

4.6. Periodic solutions

Periodic solutions of the physical problem correspond to equilibrium solutions of the modulations Eqs. (45)–(48), which are obtained by assuming that $a_x(T_2) = a_{x0}$, $a_y(T_2) = a_{y0}$, $\phi_x(T_2) = \phi_{x0}$ and $\phi_y(T_2) = \phi_{y0}$ are constants. This gives

$$0 = -cc_x a_{x0} + \frac{c_1c_4c_6(2\omega_2-1)^2+k_3}{8}\sin[2(\phi_{x0}-\phi_{y0})]a_{x0}a_{y0}^2 - \frac{F}{2}\sin(\phi_{x0}), \tag{51}$$

$$0 = -(cc_y + c_1^2cc_\alpha)\omega_2 a_{y0} - \frac{c_1c_4c_6+k_3}{8}\sin[2(\phi_{x0}-\phi_{y0})]a_{x0}^2a_{y0}, \tag{52}$$

$$0 = \frac{3k_3}{8}a_{x0}^3 + \frac{c_1c_4c_6(2\omega_2-1)^2+k_3}{8}\cos[2(\phi_{x0}-\phi_{y0})]a_{x0}a_{y0}^2 + \frac{c_1(c_3c_5+c_4c_6)+2k_3}{8}a_{x0}a_{y0}^2 - \sigma_e a_{x0} - \frac{F}{2}\cos(\phi_{x0}), \tag{53}$$

$$0 = \frac{c_1c_4c_6+k_3}{8}\cos[2(\phi_{x0}-\phi_{y0})]a_{x0}^2a_{y0} + \frac{c_1(c_3c_5+c_4c_6)+2k_3}{8}a_{x0}^2a_{y0} + \frac{2c_1^2\omega_2^2(c_1+2c_2)+3k_3}{8}a_{y0}^3 - [c_1^2I_p+(1+c_1)^2]\omega_2(\sigma_i+\sigma_e)a_{y0}, \tag{54}$$

which are four real nonlinear algebraic equations in the four real unknowns a_{x0}, a_{y0}, ϕ_{x0} and ϕ_{y0}.

From (52) and (54) it follows

$$\sin[2(\phi_{x0}-\phi_{y0})] = -\frac{8(cc_y+c_1^2cc_\alpha)\omega_2}{c_1c_4c_6+k_3}\frac{1}{a_{x0}^2}, \tag{55}$$

$$\cos[2(\phi_{x0}-\phi_{y0})] = -\frac{c_1(c_3c_5+c_4c_6)+2k_3}{c_1c_4c_6+k_3} - \frac{2c_1^2\omega_2^2(c_1+2c_2)+3k_3}{c_1c_4c_6+k_3}\frac{a_{y0}^2}{a_{x0}^2} + \frac{8[c_1^2I_p+(1+c_1)^2]\omega_2(\sigma_i+\sigma_e)}{c_1c_4c_6+k_3}\frac{1}{a_{x0}^2}. \tag{56}$$

The identities

$$\tan[2(\phi_{x0}-\phi_{y0})] = \frac{\sin[2(\phi_{x0}-\phi_{y0})]}{\cos[2(\phi_{x0}-\phi_{y0})]},$$
$$\sin[2(\phi_{x0}-\phi_{y0})]^2 + \cos[2(\phi_{x0}-\phi_{y0})]^2 = 1, \tag{57}$$

are now considered. Using (55)–(56), from $(57)_1$ it is possible to compute the phase difference $\phi_{x0}-\phi_{y0}$ once a_{x0} and a_{y0} are known. From $(57)_2$ the next equation is obtained

$$d_1a_{x0}^4 + d_2a_{y0}^4 + d_3a_{x0}^2a_{y0}^2 + d_4a_{x0}^2 + d_5a_{y0}^2 + d_6 = 0, \tag{58}$$

where the coefficients d_i, $i = 1,\dots,6$, are reported in Appendix. By means of the (58), that no longer contains $\phi_{x0}-\phi_{y0}$, it is possible to compute $a_{x0} = a_{x0}(a_{y0})$, so it is named (amplitudes) *coupling* equation. Note that it is independent of the excitation amplitude F, but depends on the excitation frequency, since the coefficients d_i, $i = 4,\dots,6$, depend on σ_e.

The unknowns are a_{x0}^2 and a_{y0}^2, and only the positive roots are of physical interest since they are amplitudes of motion. Since it is quadratic in these unknowns, it is clear that there are *at most* 2 solutions $a_{x0} = a_{x0}(a_{y0})$.

It is worth to remark that, since only two out of four equations are considered up to now, this is a necessary condition for the overall solutions, i.e. it is not yet guaranteed that all $a_{x0} = a_{x0}(a_{y0})$ actually exists. To further support this consideration, it is noted that the excitation amplitude F has not yet been considered, and the full solution of course will depend on it.

From (51) and (53) it follows

$$\sin(\phi_{x0}) = -\frac{2cc_xa_{x0}}{F} + \frac{c_1c_4c_6(2\omega_2-1)^2+k_3}{4F}\sin[2(\phi_{x0}-\phi_{y0})]a_{x0}a_{y0}^2, \tag{59}$$

$$\cos(\phi_{x0}) = \frac{3k_3}{4F}a_{x0}^3 + \frac{c_1c_4c_6(2\omega_2-1)^2+k_3}{4F}\cos[2(\phi_{x0}-\phi_{y0})]a_{x0}a_{y0}^2 + \frac{c_1(c_3c_5+c_4c_6)+2k_3}{4F}a_{x0}a_{y0}^2 - \frac{2\sigma_e a_{x0}}{F}. \tag{60}$$

Inserting in (59)–(60) the expressions of $\sin[2(\phi_{x0}-\phi_{y0})]$ and $\cos[2(\phi_{x0}-\phi_{y0})]$ given by (55) and (56) it is noted that on the right hand side there are expressions that depend on a_{x0} and a_{y0} only. Considering the following identities:

$$\tan(\phi_{x0}) = \frac{\sin(\phi_{x0})}{\cos(\phi_{x0})},$$
$$\sin(\phi_{x0})^2 + \cos(\phi_{x0})^2 = 1, \tag{61}$$

and using (59) and (60), from $(61)_1$ it is obtained ϕ_{x0} as a function of a_{x0} and a_{y0}, while from $(61)_2$ the following equation is obtained

$$e_1a_{x0}^8 + e_2a_{x0}^6a_{y0}^2 + e_3a_{x0}^4a_{y0}^4 + e_4a_{x0}^2a_{y0}^6 + e_5a_{y0}^8 + e_6a_{x0}^6 + e_7a_{x0}^4a_{y0}^2 + e_8a_{x0}^2a_{y0}^4 + e_9a_{y0}^6 + e_{10}a_{x0}^4 + e_{11}a_{x0}^2a_{y0}^2 + e_{12}a_{y0}^4 = 16F^2(c_1c_4c_6+k_3)^2a_{x0}^2, \tag{62}$$

where the coefficients e_i, $i = 1,\dots,12$, have long expressions that are reported in Appendix. It is quartic in the unknowns a_{x0}^2 and a_{y0}^2, and thus there are *at most* 4 solutions $a_{x0} = a_{x0}(a_{y0})$, that depend on the excitation amplitude F.

Summarizing, giving all the parameters (and in particular F and σ_e, i.e. amplitude and frequency of the external excitation), it is possible to solve the two nonlinear algebraic Eqs. (58) and (62), and to compute a_{x0} and a_{y0}; note that, according to the nonlinear nature of problem, multiple solutions may exist for the same parameters (examples will the reported in the following), up to $2\times4 = 8$. Then, for each solution of (58) and (62), ϕ_{x0} and ϕ_{y0} are computed by means of $(57)_1$ and $(61)_1$, and then $x(t)$, $y(t)$ and $\alpha(t)$ are known, up to the second order.

Before ending this subsection, it is noted that the single mode along-wind solution ($a_{y0} = 0$) is simply given by

$$\sin(\phi_{x0}) = -\frac{2cc_xa_{x0}}{F},$$
$$\cos(\phi_{x0}) = a_{x0}\frac{3k_3a_{x0}^2 - 8\sigma_e}{4F}, \tag{63}$$

from which

$$\sigma_e = \frac{3}{8}k_3a_{x0}^2 \pm \frac{\sqrt{F^2-4cc_x^2a_{x0}^2}}{2a_{x0}}. \tag{64}$$

From the previous expressions a_{x0} and ϕ_{x0} can be easily determined. Since $a_{y0} = 0$, it remains to compute ϕ_{y0}, which is a solution of

$$\cos[2(\phi_{x0}-\phi_{y0})] = f,$$
$$f = -\frac{c_1(c_3c_5+c_4c_6)+2k_3}{c_1c_4c_6+k_3} + \frac{8[c_1^2I_p+(1+c_1)^2]\omega_2(\sigma_i+\sigma_e)}{c_1c_4c_6+k_3}\frac{1}{a_{x0}^2}, \tag{65}$$

that comes from (56). Two different cases may occur:

- $|f| \le 1$. In this case ϕ_{y0} exists and can be computed by (65);
- $|f| > 1$. In this case (65) is impossible, and thus no ϕ_{y0} exists. The dynamics of $\phi_y(T_2)$ is then governed by (50). This situation has only a mathematical interest, since for $a_y = 0$ the behaviour of ϕ_y is unessential from an engineering point of view, see (44).

4.7. Stability and bifurcations

To study the stability of the solutions obtained in Section 4.6 it is necessary to solve the Eqs. (45)–(48) with respect to their derivates (only the first one is already in this format), and then to compute the gradient $\hat{G}$ of the right hand side, which is a 4×4 matrix, in correspondence of a_{x0}, a_{y0}, ϕ_{x0} and ϕ_{y0}. This can be easily done, but it is not reported since the expressions are very long and complex. In the single mode along-wind case $a_y = 0$ it simplifies to:

$$\hat{G} = \begin{bmatrix} -cc_x & 0 & -\frac{F}{2}\cos(\phi_x) & 0 \\ 0 & G_{22} & 0 & 0 \\ \frac{3}{4}k_3a_x + \frac{F}{2}\frac{\cos(\phi_x)}{a_x^2} & 0 & \frac{F}{2}\frac{\sin(\phi_x)}{a_x} & 0 \\ G_{41} & 0 & -G_{44} & G_{44} \end{bmatrix}, \tag{66}$$

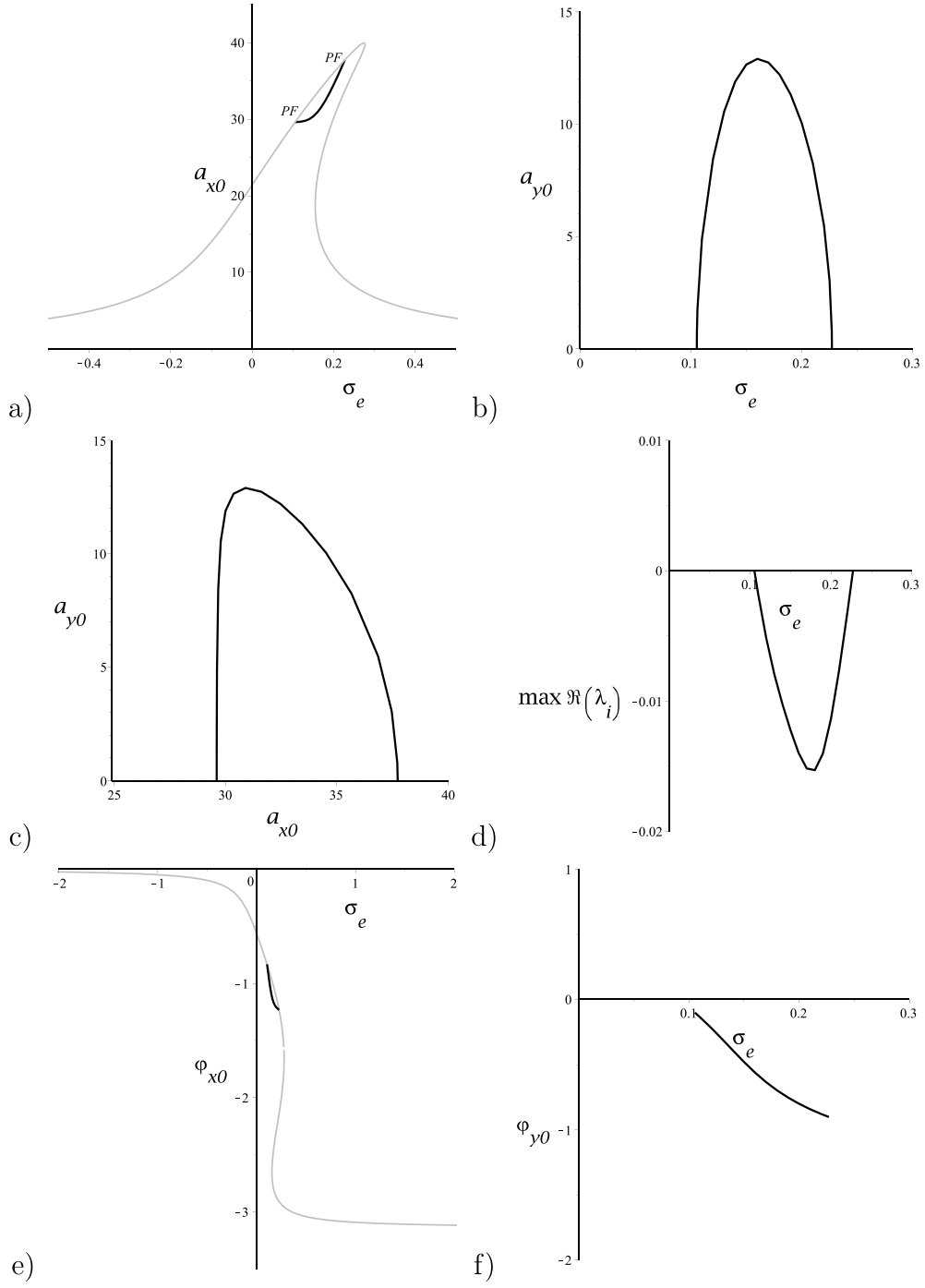

Fig. 2. The analytical solution paths for $F = 4$. Grey is the single mode along-wind solution, black the along-wind and cross-wind coupled *stable* solution.

Table 1
The mechanical parameters of the NREL 5-MW reference wind turbine.

parameter	value	dimension
H	90	m
d	1.9	m
M	523730	kg
$\bar{I}_p$	3.94857×10^6	kg m^2
ν (steel)	0.3	

where the expressions of G_{22}, G_{14} and G_{34} are reported in Appendix.

The stability is determined by the four eigenvalues λ_i of $\hat{G}$:

- If *all* λ_i have real part lesser than zero, then the physical periodic solution is stable;
- If *at least* one λ_i has a real part larger than zero, than the physical periodic solution is unstable.

Thus, the stability is governed by the sign of $\max Re(\lambda_i)$.

By varying one (or more) parameter of the system, the transition from stability to instability occurs at $\max Re(\lambda_i) = 0$, which is then the condition to have a *bifurcation*.

There are different types of bifurcations: if, when $\max Re(\lambda_i) = 0$, also $Im(\lambda_i) = 0$ (namely the eigenvalue is real), then a SN or PF bifurcation occurs; if, on the other hand, $Im(\lambda_i) \neq 0$, a NS bifurcation happens, and at a physical level a quasi-periodic solution appears. All these cases are seen to occur in Section 5.

A special attention deserves the stability of the single mode along-wind solution. The four eigenvalues of (66) are (use is made of (63))

$$\lambda_1 = \frac{(c_1c_4c_6 + k_3)\sin[2(\phi_{x0} - \phi_{y0})]}{4\omega_2[c_1^2 I_p + (1+c_1)^2]} a_{x0}^2,$$
$$\lambda_{2,3} = -cc_x \pm \frac{1}{8}\sqrt{-(3k_3a_{x0}^2 - 8\sigma_e)(9k_3a_{x0}^2 - 8\sigma_e)},$$
$$\lambda_4 = -\frac{(c_1c_4c_6 + k_3)\sin[2(\phi_{x0} - \phi_{y0})]a_{x0}^2 + 8\omega_2(c_1^2 cc_\alpha + cc_y)}{8\omega_2[c_1^2 I_p + (1+c_1)^2]}. \quad (67)$$

Looking for along-wind and cross-wind *coupled* solutions branching from the single mode along-wind one, it is needed to solve (58) and (62) for $a_{y0} = 0$:

$$d_1 a_{x0}^4 + d_4 a_{x0}^2 + d_6 = 0,$$
$$9k_3^2 a_{x0}^6 - 48k_3\sigma_e a_{x0}^4 + 64(cc_x^2 + \sigma_e^2)a_{x0}^2 = 16\,F^2. \quad (68)$$

Note that the latter can also be obtained directly by (63). Given F, these are two equations in the two unknowns a_{x0} and σ_e, that determine the branching point from the single mode along-wind solution, which is of major interest for this study.

Long but simple computations show that in the correspondence of this branching point $\lambda_4 = 0$, in perfect agreement with the fact that it is a bifurcation point. Actually, it corresponds to a PF bifurcation, since the branched solution depends on a_{y0}^2 and thus it is symmetric with respect to the set $a_{y0} = 0$ (see forthcoming Fig. 2c).

5. Results

To illustrate the previous findings the NREL 5-MW reference wind turbine [43] is considered. It has the mechanical properties reported in Table 1 and has been used, among other, also in [27,30,34].

The expressions obtained in Section 2 give the dimensionless parameters of Table 2, where the selected damping coefficients are also reported. From the previous values the parameters reported in Table 3 follow. Note that σ_i is very small, and thus close to the perfect 1:1 internal resonance $\sigma_i = 0$.

For $F < 3.677728$ there are no branching solutions, and only the along-wind vibration occurs. Slightly above, the solution for $F = 4$ is reported in Figs. 2 and 3.

Table 2
The dimensionless parameters of the considered Wind Turbine.

parameter	value
k_3	0.00045841
k_α	1725.974856
I_p	2.08846
cc_x	0.05
cc_y	0.05
cc_α	0.05

Table 3
The parameters considered in the reference example.

parameter	value
ω_2	0.99971
ω_3	28.7561
σ_i	0.000289916
c_1	0.00058008422
c_2	2.24375×10^{-7}
c_3	4.49994
c_4	$-2.824886 \times 10^{-14}$
c_3c_5	-3.37463×10^{-7}
c_4c_6	-3.36091×10^{-7}

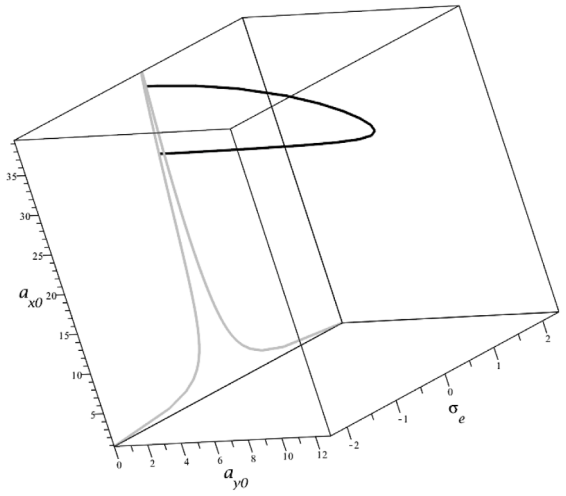

Fig. 3. A 3D illustration of the single mode (grey) and coupled branching (black) solutions for $F = 4$.

The branching from the single mode along-wind solution is quite evident, and occurs by a PF bifurcation at $a_{x0} = 29.616295$ and $\sigma_e = 0.105391$. The branched solution is always stable, and reconnects to the single mode solution in another (reverse) PF bifurcation at $a_{x0} = 37.731845$ and $\sigma_e = 0.227144$. In between the two PFs, the single mode along-wind solution is unstable, and this is the most important, and dangerous, effect of the coupling. The safety limit is that in correspondence of the first PF, which is lower than the peak of the FRC of the single mode solution, at $a_{x0} = 40$, that in principle could be reached without the coupling due to the internal resonance.

A more involved, and more unsafe, situation occurs for increasing excitation amplitude. For $F = 7$ the solution is reported in Figs. 4 and 5.

The PF bifurcation occurs at $a_{x0} = 32.525846$ and $\sigma_e = 0.086578$, and by increasing σ_e the branched solution undergoes a reverse SN bifurcation at $a_{x0} = 35.6902605$ and $\sigma_e = 0.30203$, where it loses stability. The path then continues for decreasing σ_e, up to another SN at $a_{x0} = 30.760698$ and $\sigma_e = 0.28978$ where it regains stability. Soon after, at $a_{x0} = 29.537844$ and $\sigma_e = 0.301$ it undergoes a NS bifurcation, where it loses again stability (this stable path is very short and barely

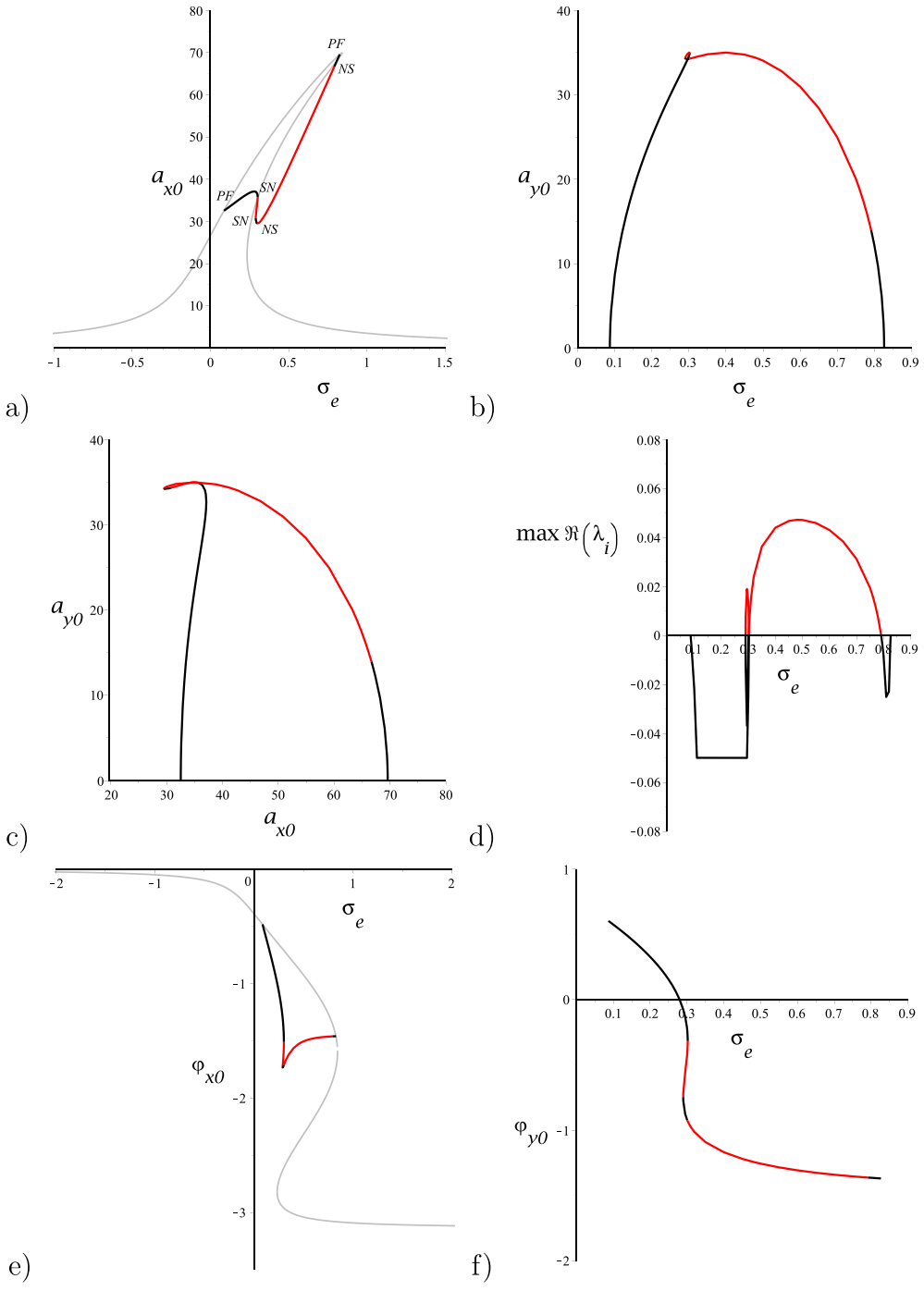

Fig. 4. The analytical solution paths for $F = 7$. Grey is the single mode along-wind solution, black the along-wind and cross-wind coupled *stable* solution, red the along-wind and cross-wind coupled *unstable* solution.

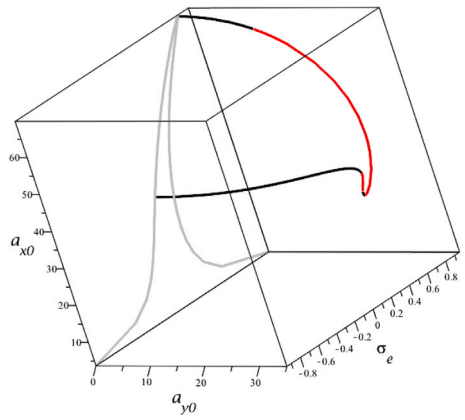

Fig. 5. A 3D illustration of the single mode (grey), coupled branching *stable* (black) and coupled branching *unstable* (red) solutions for $F = 7$.

visible in Fig. 4), up to another NS bifurcation at $a_{x0} = 66.6643045$ and $\sigma_e = 0.7915$. Between the two NS bifurcations the system undergoes a quasi-periodic along-wind and across-wind coupled oscillation, which is particularly risky in terms of durability due to fatigue; an example is reported in forthcoming Fig. 11. The final stable path reconnects to the single mode solution by a reverse PF bifurcation at $a_{x0} = 69.572440$ and $\sigma_e = 0.826523$, just below the peak of the FRC that occurs at $a_{x0} = 70$ and $\sigma_e = 0.842333$.

By further increasing the excitation amplitude the qualitative behaviour does not change significantly, even if the branching path is more wavy (see Figs. 6 and 7 for $F = 10$).

As already mentioned, and as it is clear from the previous pictures, the critical threshold that cannot be overcome for safety is given by the first PF bifurcation, where the branching coupled solution is born. In Fig. 8 it is reported how this limit depends on F. For comparison, the value of the second reverse PF (in red) and of the peak of the FRG (dashed black) are also reported. This latter can be computed by (64) and is given by

$$a_{x0,cr} = \frac{F}{2cc_x}, \qquad \sigma_{e,cr} = \frac{3k_3F^2}{32cc_x^2}. \tag{69}$$

They almost coincide.

It is noted that the critical threshold is slowly increasing for varying F, which is easier to reach for large excitation amplitudes and thus is very dangerous. For $F < 3.677728$ the critical threshold is the peak point of the FRC.

To end this section it is worth to remark that coupled solutions that do not branch from the single mode solution, i.e. *isolated* coupled solutions, have not been found. However, it cannot be excluded that they exist for different values of the parameters, i.e. for different wind turbine towers.

5.1. Comparison with numerical simulations

To check the analytical approximate solution it is compared with some numerical solutions of the governing Eqs. (9)–(11), or better (12)–(14). To have reliable results, numerical solutions are obtained both by a self-made code in C++ and by using a software with built-in algorithms for numerical solutions of ODEs.

An example is reported in Fig. 9 for $F = 7$ and $\sigma_e = 0.17$. An excellent agreement is observed, both at qualitative and quantitative level, for the along-wind x and cross-wind y oscillations. For the rotation α, that as expected has a smaller amplitude, the first order solution is not accurate enough because of the non harmonic behaviour of α. However, it captures the order of magnitude of the rotation amplitude, and thus it is in any case useful from an engineering point of view.

To further check the analytical solution, the bifurcation diagram for $F = 10$ is reported in Fig. 10. It has been obtained by a brute-force algorithm, and so it reports only the stable solutions.

Comparing Fig. 10 with its counterpart Fig. 6 it is observed that there is an excellent agreement between numerical and analytical results, which is further confirmed quantitatively by the fact that PF bifurcation occurs at $\sigma_{e,cr} = 0.093236$ and $a_{x0,cr} = 36.001482$ (analytical) versus $\sigma_{e,cr} = 0.09$ and $a_{x0,cr} = 36.31$ (numerical).

The excellent agreement between the analytical and numerical evaluations of the PF critical threshold holds for all values of F, as can be seen in Fig. 8, where the blue and black curves are practically undistinguishable. This is a robust check of the reliability of the proposed analytical solution for detecting the born and the occurrence of along-wind and cross-wind coupled oscillations.

Remarkably, in part of the unstable branch of Fig. 10, the numerical solution is a quasi-periodic motion, as expected after a NS bifurcation. An example of this latter is reported in Fig. 11, where the quasi-periodicity is confirmed by the fact that the Poincaré points lay on a closed curve.

6. Conclusions

The along-wind and cross-wind coupled oscillations in the nonlinear dynamics of a wind turbine tower have been investigated in correspondence with the 1:1 internal resonance due to the axial-symmetric cross-section of the column.

A three dof simplified model has been initially obtained, taking into account the two horizontal translations and the rotation around the vertical axis of the wind turbine tower.

After having introduced dimensionless equations, that are easier to handle without loss of generality, an analytical approximation of the nonlinear oscillations has been obtained using the MTSM, taking into account internal and external resonances, which are the worst cases and thus of major relevance for applications.

The solution has been obtained by solving two algebraic nonlinear equations, one of the second order and the other of the fourth order. Thus, the solution can be easily obtained.

Although the proposed solution is valid for any wind turbine tower, the NREL 5-MW reference wind turbine, which is frequently considered in the renewable energy research field, has been used as an example.

The existence of an along-wind and cross-wind coupled solution branching from the single mode along-wind solution, through a PF bifurcation, has been shown. A parametric analysis obtained by varying the frequency of the external excitation (the oscillating part of the wind) has been reported, and the related FRCs have been illustrated. It has been shown how the coupled solution changes by increasing the excitation amplitude, and how it can have a quite complex behaviour and can lose stability by SN and NS bifurcations.

Attention has been focused on the branching point, which is the critical limit for the safe use of the wind turbine system. It has been shown that it weakly depends on the excitation amplitude.

The approximate analytical solution has been compared with numerical simulations to check its reliability. A very good agreement has been observed, suggesting that the proposed solution can be profitably used for the analysis and design of wind turbine systems.

Although in the work reference is explicitly made to the force due to the wind, the proposed model is able to consider also the excitation coming from the sea waves (and mooring lines) in FOWT: It is sufficient to add on the right-hand side of (5)–(7) the translation and rotational inertia due to the motion of the buoy, and the same analysis applies. The same is true for earthquake excitations.

It is hoped that, once further deeply investigated and fully understood, this phenomenon will be properly considered by the wind industry and by the related policymakers.

The proposed study is based on various hypotheses (i) on the mechanical model (a 3 dof system is considered and no other higher

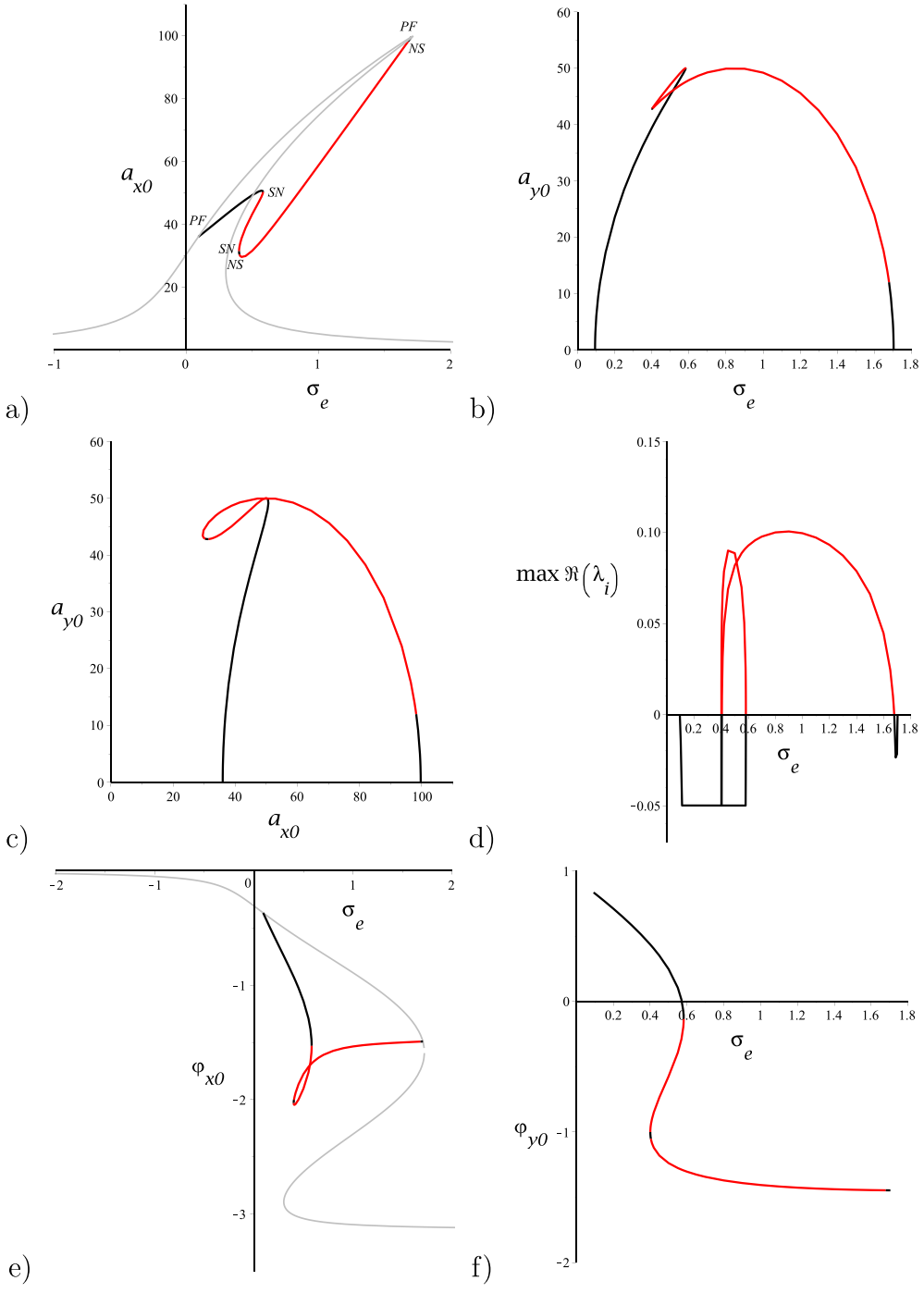

Fig. 6. The analytical solution paths for $F = 10$. Grey is the single mode along-wind solution, black the along-wind and cross-wind coupled *stable* solution, red the along-wind and cross-wind coupled *unstable* solution.

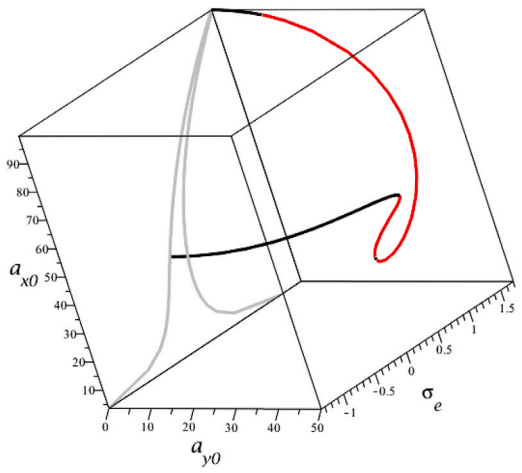

Fig. 7. A 3D illustration of the single mode (grey), coupled branching *stable* (black) and coupled branching *unstable* (red) solutions for $F = 10$.

order normal modes of the tower are included, no vertical motion of the nacelle is considered, the excitation is harmonic, the rotation has no nonlinearities, no interactions with the blades has been taken into account, etc.) and (ii) on the solution (the amplitude is not large so that the third order MTSM solution is reliable). Although all of them look realistic, further development consists of checking what will happen when these assumptions are relaxed, in particular if coupled solutions still exist. It is not expected that this can be done analytically since the model will become much more complex, and it will require the heavy use of numerical simulations, thus losing the simplicity and generality of the proposed approach.

In addition to the previous one, another development is absolutely needed, namely the comparison of the proposed findings with experimental data coming from monitoring of real (or laboratory) wind turbine towers, to assess the relevance of the investigated phenomenon. Very preliminary checks look promising (Fig. 2 A of [49] shows the same qualitative behaviour illustrated in Fig. 9d), but a systematic comparison is necessary and left for future works.

CRediT authorship contribution statement

Stefano Lenci: Conceptualization, Methodology, Software, Data curation, Writing, Visualization, Investigation, Validation, Writing – review & editing.

Declaration of competing interest

The authors declare that they have no known competing financial interests or personal relationships that could have appeared to influence the work reported in this paper.

Data availability

Data will be made available on request.

Acknowledgements

This work has been partially developed within the COST ACTION "CA20109 MODENERLANDS". The financial support of the PRIN 2022 project "NonlinEar Phenomena in floaTing offshore wind tUrbiNEs (NEPTUNE)", prot. 2022W7SKTL, is greatly acknowledged.

Appendix

The expressions of various parameters used in the text are reported in the following.

$$c_1 = -1 + \frac{1}{\omega_2^2}. \tag{A.1}$$

$$\begin{aligned}
c_2 &= 2\frac{(\omega_2^2-1)^2}{\omega_2^2(4\omega_2^2-1)},\\
c_3 &= \frac{(\omega_2^2-1)^3}{\omega_2^2[\omega_2(\omega_2+2)(\omega_2+1)^2 I_p - \omega_2(\omega_2+2)k_\alpha - (\omega_2+1)^2]},\\
c_4 &= \frac{(\omega_2^2-1)^3}{\omega_2^2[\omega_2(\omega_2-2)(\omega_2-1)^2 I_p - \omega_2(\omega_2-2)k_\alpha - (\omega_2-1)^2]},\\
c_5 &= -\frac{\omega_2(\omega_2+2)}{(\omega_2+1)^2},\\
c_6 &= -\frac{\omega_2(\omega_2-2)}{(\omega_2-1)^2}.
\end{aligned} \tag{A.2}$$

$$\begin{aligned}
H_1 &= -\left[c_1c_3c_5A_xA_y^2(2\omega_2+1)^2e^{-2I\sigma_iT_2} + k_3A_x(A_x^2+A_y^2e^{-2I\sigma_iT_2})\right],\\
H_2 &= -\left[2I\frac{\partial A_x}{\partial T_2} + 2Icc_xA_x + (c_1c_4c_6(2\omega_2-1)^2\bar{A}_xA_y^2)e^{-2I\sigma_iT_2}\right.\\
&\quad + c_1(c_3c_5+c_4c_6)A_xA_y\bar{A}_y + (3A_x^2\bar{A}_x + 2A_xA_y\bar{A}_y + \bar{A}_xA_y^2e^{-2I\sigma_iT_2})k_3\\
&\quad \left.-\frac{F}{2}e^{I\sigma_eT_2}\right],\\
H_3 &= -\left[\frac{3}{2}c_1^3\omega_2^2A_y^3 + k_3A_y(A_y^2+A_x^2e^{2I\sigma_iT_2})\right],\\
H_4 &= -\left[2(1+c_1)I\omega_2\frac{\partial A_y}{\partial T_2} + 2Icc_y\omega_2A_y + \frac{1}{2}c_1^3\omega_2^2A_y^2\bar{A}_y\right.\\
&\quad \left.k_3\left(2A_x\bar{A}_xA_y + 3A_y^2\bar{A}_y + A_x^2\bar{A}_ye^{2I\sigma_iT_2}\right)\right],\\
H_5 &= -\left[c_1\omega_2^2\left(\frac{c_1}{2}+4c_2\right)A_y^3 + c_3c_5A_x^2A_ye^{2I\sigma_iT_2}\right],\\
H_6 &= -\left[2I(1+c_1(1+I_p))\omega_2\frac{\partial A_y}{\partial T_2} + 2Icc_\alpha c_1\omega_2A_y\right.\\
&\quad \left.+\frac{1}{2}c_1\omega_2^2(3c_1+8c_2)A_y^2\bar{A}_y + c_4c_6A_x^2\bar{A}_ye^{2I\sigma_iT_2} + (c_4c_6+c_3c_5)A_x\bar{A}_xA_y\right].
\end{aligned} \tag{A.3}$$

$$\begin{aligned}
d_1 &= (c_1c_3c_5+k_3)[c_1(c_3c_5+2c_4c_6)+3k_3],\\
d_2 &= [2c_1^2\omega_2^2(c_1+2c_2)+3k_3]^2,\\
d_3 &= 2[c_1(c_3c_5+c_4c_6)+2k_3][2c_1^2\omega_2^2(c_1+2c_2)+3k_3],\\
d_4 &= -16\omega_2(\sigma_e+\sigma_i)[c_1(c_3c_5+c_4c_6)+2k_3][c_1^2I_p+(1+c_1)^2],\\
d_5 &= -16\omega_2(\sigma_e+\sigma_i)[2c_1^2\omega_2^2(c_1+2c_2)+3k_3][c_1^2I_p+(1+c_1)^2],\\
d_6 &= 64\omega_2^2[(\sigma_e+\sigma_i)^2[c_1^2I_p+(1+c_1)^2]^2+(c_1^2cc_\alpha+cc_y)^2].
\end{aligned} \tag{A.4}$$

$$\begin{aligned}
e_1 &= 9k_3^2(c_1c_4c_6+k_3)^2,\\
e_2 &= -24c_1c_4c_6k_3\omega_2(\omega_2-1)(c_1c_4c_6+k_3)[c_1(c_3c_5+c_4c_6)+2k_3],\\
e_3 &= -12c_4^2c_6^2k_3\omega_2^2(2\omega_2-1)^2c_1^5\\
&\quad - 8c_4c_6\omega_2^2[3(2\omega_2^2-2\omega_2+1)k_3^2 + 3c_2c_4c_6(2\omega_2-1)^2k_3\\
&\quad - 2c_4c_6(\omega_2-1)^2(c_3c_5+c_4c_6)^2]c_1^4\\
&\quad - 4k_3\omega_2^2[3k_3^2 + 12c_2c_4c_6(2\omega_2^2-2\omega_2+1)k_3\\
&\quad - 16c_4^2c_6^2(\omega_2-1)^2(c_3c_5+c_4c_6)]c_1^3\\
&\quad - 2k_3^2[-32c_4^2c_6^2\omega_2^3(\omega_2-2) + (4c_4^2c_6^2+12c_2k_3)\omega_2^2 - 9c_4^2c_6^2(4\omega_2-1)]c_1^2\\
&\quad - 36c_4c_6k_3^3(2\omega_2^2-2\omega_2+1)c_1 - 18k_3^4,\\
e_4 &= 8c_1c_4c_6\omega_2(\omega_2-1)(c_1c_4c_6(2\omega_2-1)^2+k_3)(c_1(c_3c_5+c_4c_6)+2k_3)\\
&\quad \times (2c_1^2\omega_2^2(c_1+2c_2)+3k_3),\\
e_5 &= (c_1c_4c_6(2\omega_2-1)^2+k_3)^2(2c_1^2\omega_2^2(c_1+2c_2)+3k_3)^2,\\
e_6 &= -48k_3\sigma_e(c_1c_4c_6+k_3)^2,
\end{aligned}$$

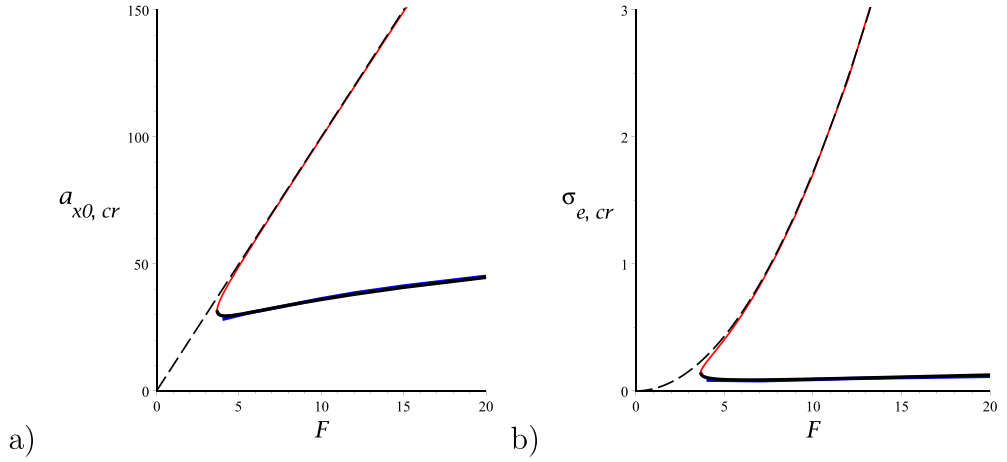

Fig. 8. (a) The critical threshold (black curve), corresponding to the first PF bifurcation, as a function of F. For comparison are also reported the peak values (dashed curves), the second reverse PF bifurcation (red) and the numerically obtained PF (blue, almost undistinguishable from the theoretical one).

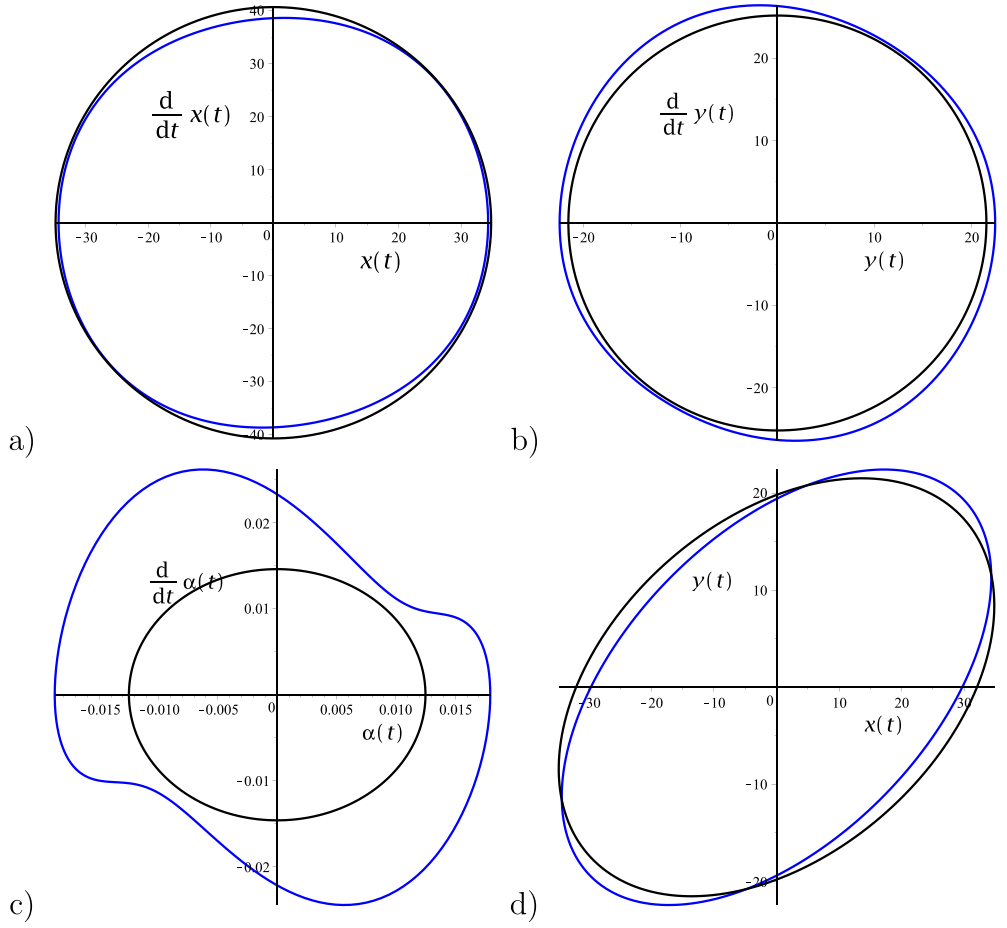

Fig. 9. The phase space trajectories of the first order analytical (black) and numerical (blue) solutions for $F = 7$ and $\sigma_e = 0.17$.

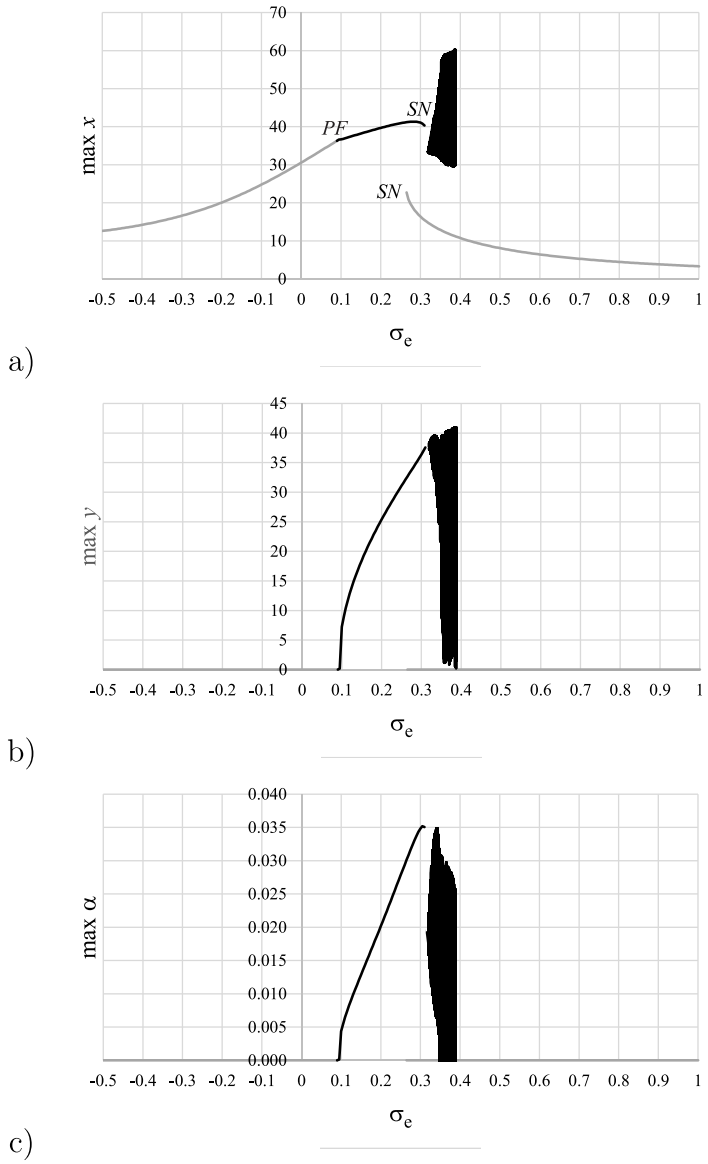

Fig. 10. The numerical solution paths for $F = 10$. Grey is the single mode along-wind solution, black the along-wind and cross-wind coupled *stable* solution.

$$
\begin{aligned}
e_7 &= 16\omega_2(c_1c_4c_6k_3)[3c_4c_6k_3(2\omega_2-1)^2(\sigma_e+\sigma_i)(1+I_p)c_1^3\\
&+ (24c_4c_6k_3(\sigma_e+\sigma_i)\omega_2^2 + 4c_4c_6((c_3c_5+c_4c_6)\sigma_e - 6k_3(\sigma_e+\sigma_i)\\
&+ 3(\sigma_e+\sigma_i)(1+I_p)k_3^2 + 6c_4c_6(\sigma_e+\sigma_i)k_3 - c_4c_6\sigma_e(c_3c_5+c_4c_6))\omega_2)c_1^2\\
&k_3(12c_4c_6(\sigma_e+\sigma_i)\omega_2^2 - 4c_4c_6(\sigma_e+3\sigma_i)\omega_2 - c_4c_6(5\sigma_e-3\sigma_i)\\
&+ 6k_3(\sigma_e+\sigma_i))c_1 + 3k_3^2(\sigma_e+\sigma_i)],\\
e_8 &= -16(c_1c_4c_6(2\omega_2-1)^2+k_3)[2c_4c_6\omega_2^2(2(\sigma_e+\sigma_i)(c_3c_5+c_4c_6)(1+I_p)\omega_2\\
&- 2(\sigma_e+\sigma_i)(c_3c_5+c_4c_6)(1+I_p) - \sigma_e)c_1^4\\
&+ 2\omega_2^2(4c_4c_6(\sigma_e+\sigma_i)(c_3c_5+c_4c_6+k_3(1+I_p))\omega_2\\
&- (4c_4c_6(\sigma_e+\sigma_i)(1+I_p)+\sigma_e)k_3\\
&- 2c_4c_6(2(\sigma_e+\sigma_i)(c_3c_5+c_4c_6)+c_2\sigma_e))c_1^3\\
&- 4\omega_2^2(-c_4c_6(\sigma_e+\sigma_i)(c_3c_5+c_4c_6+4k_3)\omega_2\\
&+ (4c_4c_6(\sigma_e+\sigma_i)+c_2\sigma_e)k_3 + c_4c_6(\sigma_e+\sigma_i)(c_3c_5+c_4c_6))c_1^2\\
&+ c_4c_6k_3(8\omega_2^2(\sigma_e+\sigma_i)(\omega_2-1) - 3\sigma_e)c_1 - 3k_3^2\sigma_e],\\
e_9 &= -16\omega_2(c_1c_4c_6(2\omega_2-1)^2+k_3)^2(\sigma_e+\sigma_i)(2c_1^2\omega_2^2(c_1+2c_2)+3k_3)\\
&\times (c_1^2I_p + (1+c_1)^2),\\
e_{10} &= 64(cc_x^2+\sigma_e^2)(c_1c_4c_6+k_3)^2,\\
e_{11} &= -128\omega_2(c_1c_4c_4+k_3)(c_1c_4c_6(2\omega_2-1)^2+k_3)\\
&\times (\sigma_e(\sigma_e+\sigma_i)(c_1^2I_p+(1+c_1)^2) - cc_x(c_1^2cc_\alpha+cc_y)),\\
e_{12} &= 64\omega_2^2(c_1c_4c_6(2\omega_2-1)^2+k_3)^2\\
&\times ((\sigma_e+\sigma_i)^2(c_1I_p^2+(1+c_1)^2)^2 + (c_1^2cc_\alpha+cc_y)^2).
\end{aligned}
\tag{A.5}
$$

$$
\begin{aligned}
G_{22} &= -\frac{(c_1c_4c_6+k_3)\sin[2(\phi_x-\phi_y)]a_x^2 + 8\omega_2(c_1^2cc_\alpha+cc_y)}{8\omega_2[c_1^2I_p+(1+c_1)^2]},\\
G_{41} &= \frac{(c_1c_4c_6+k_3)\cos[2(\phi_x-\phi_y)] + c_1(c_3c_5+c_4c_6)+2k_3}{4\omega_2[c_1^2I_p+(1+c_1)^2]}a_x,\\
G_{44} &= \frac{(c_1c_4c_6+k_3)\sin[2(\phi_x-\phi_y)]}{4\omega_2[c_1^2I_p+(1+c_1)^2]}a_x^2.
\end{aligned}
\tag{A.6}
$$

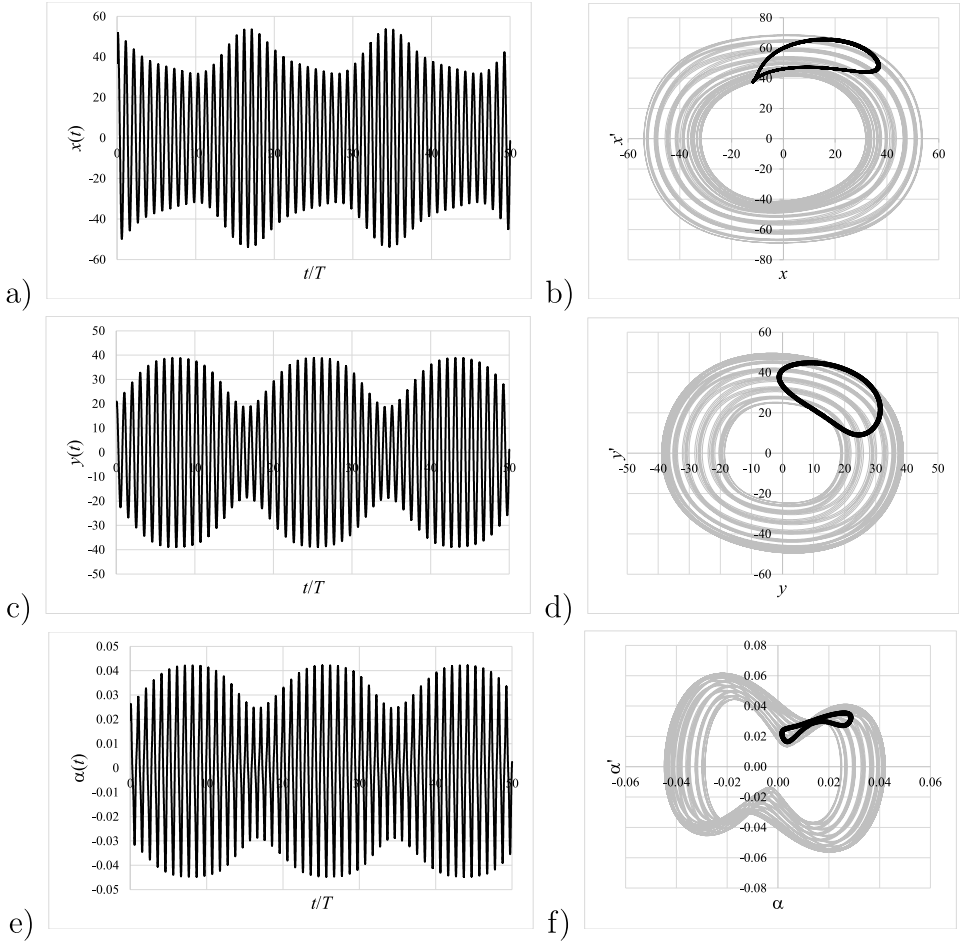

Fig. 11. The numerical quasi-periodic solution for $F = 10$ and $\sigma_e = 0.35$, so that $T = 2\pi/\omega = 2\pi/(1+\sigma_e) = 4.6542$. (a), (c) and (e) time history of $x(t)$, $y(t)$ and $\alpha(t)$. (b), (d) and (e) phase portraits (grey) and Poincaré map points (black) of $x(t)$, $y(t)$ and $\alpha(t)$.

References

[1] Green new deal. 2019, URL https://commission.europa.eu/strategy-and-policy/priorities-2019-2024/european-green-deal/delivering-european-green-deal_en.

[2] Lee J, Zhao F. Global wind report. Tech. rep., Global Wind Energy Council; 2021.

[3] Future of wind: Deployment, investment, technology, grid integration and socio-economic aspects (A Global Energy Transformation paper). Tech. rep., International Renewable Energy Agency (IRENA); 2019.

[4] Renewable energy. 2021, Office of Energy Efficiency & Renewable Energy, URL https://www.energy.gov/eere/renewable-energy.

[5] Patel YR. FSI in wind turbines: A review. Int J Recent Contrib Eng Sci IT (iJES) 2020;8(3):37–50. http://dx.doi.org/10.3991/ijes.v8i3.16595.

[6] Roul R, Kumar A. Fluid-structure interaction of wind turbine blade using four different materials: Numerical investigation. Symmetry 2020;12(9). http://dx.doi.org/10.3390/sym12091467.

[7] Hsu M, Bazilevs Y. Fluid–structure interaction modeling of wind turbines: Simulating the full machine. Comput Mech 2012;50:821–33. http://dx.doi.org/10.1007/s00466-012-0772-0.

[8] Wang L, Quant R, Kolios A. Fluid structure interaction modelling of horizontal-axis wind turbine blades based on CFD and FEA. J Wind Eng Ind Aerodyn 2016;158:11–25. http://dx.doi.org/10.1016/j.jweia.2016.09.006.

[9] Grinderslev C, González Horcas S, Sørensen NN. Fluid–structure interaction simulations of a wind turbine rotor in complex flows, validated through field experiments. Wind Energy 2021;24(12):1426–42. http://dx.doi.org/10.1002/we.2639.

[10] Micallef D, Rezaeiha A. Floating offshore wind turbine aerodynamics: Trends and future challenges. Renew Sustain Energy Rev 2021;152:111696. http://dx.doi.org/10.1016/j.rser.2021.111696.

[11] Otter A, Murphy J, Pakrashi V, Robertson A, Desmond C. A review of modelling techniques for floating offshore wind turbines. Wind Energy 2022;25(5):831–57. http://dx.doi.org/10.1002/we.2701.

[12] Chen P, Chen J, Hu Z. Review of experimental-numerical methodologies and challenges for floating offshore wind turbines. J Mar Sci Appl 2018;122:576–88. http://dx.doi.org/10.1007/s11804-020-00165-z.

[13] Subbulakshmi A, Verma M, Keerthana M, Sasmal S, Harikrishna P, Kapuria S. Recent advances in experimental and numerical methods for dynamic analysis of floating offshore wind turbines — An integrated review. Renew Sustain Energy Rev 2022;164:112525. http://dx.doi.org/10.1016/j.rser.2022.112525.

[14] Xie F, Aly A-M. Structural control and vibration issues in wind turbines: A review. Eng Struct 2020;210:110087. http://dx.doi.org/10.1016/j.engstruct.2019.110087.

[15] Gkantou M, Rebelo C, Baniotopoulos C. Life Cycle Assessment of tall onshore hybrid steel wind turbine towers. Energies 2020;13(15). http://dx.doi.org/10.3390/en13153950.

[16] Agarwal P, Manuel L. Simulation of offshore wind turbine response for long-term extreme load prediction. Eng Struct 2009;31(10):2236–46. http://dx.doi.org/10.1016/j.engstruct.2009.04.002.

[17] Marino E, Nguyen H, Lugni C, Manuel L, Borri C. Irregular nonlinear wave simulation and associated loads on offshore wind turbines. J Offshore Mech Arct Eng 2015;137(2). http://dx.doi.org/10.1115/1.4029212, 021901.

[18] Veljkovic M, Feldmann M, Naumes J, Pak D, Simões L, da Silva L, Rebelo C. 9 - wind turbine tower design, erection and maintenance. In: Sørensen JD, Sørensen JN, editors. Wind energy systems. Woodhead publishing series in energy, Woodhead Publishing; 2011, p. 274–300. http://dx.doi.org/10.1533/9780857090638.2.274.

[19] Malliotakis G, Alevras P, Baniotopoulos C. Recent advances in vibration control methods for wind turbine towers. Energies 2021;14(22). http://dx.doi.org/10.3390/en14227536.

[20] Yang J, Fang L, Song D, Su M, Yang X, Huang L, et al. Review of control strategy of large horizontal-axis wind turbines yaw system. Wind Energy 2021;24(2):97–115. http://dx.doi.org/10.1002/we.2564.

[21] Yang B, Sun D. Testing, inspecting and monitoring technologies for wind turbine blades: A survey. Renew Sustain Energy Rev 2013;22:515–26. http://dx.doi.org/10.1016/j.rser.2012.12.056.

[22] Ma Y, Martinez-Vazquez P, Baniotopoulos C. Buckling analysis for wind turbine tower design: Thrust load versus compression load based on energy method. Energies 2020;13(20). http://dx.doi.org/10.3390/en13205302.

[23] Zuo H, Bi K, Hao H. A state-of-the-art review on the vibration mitigation of wind turbines. Renew Sustain Energy Rev 2020;121:109710. http://dx.doi.org/10.1016/j.rser.2020.109710.
[24] Liao D, Zhu S-P, Correia JA, De Jesus AM, Veljkovic M, Berto F. Fatigue reliability of wind turbines: Historical perspectives, recent developments and future prospects. Renew Energy 2022;200:724–42. http://dx.doi.org/10.1016/j.renene.2022.09.093.
[25] Dagli BY, Tuskan Y, Gokkus U. Evaluation of offshore wind turbine tower dynamics with numerical analysis. Adv Civ Eng 2018;2018:3054851. http://dx.doi.org/10.1155/2018/3054851.
[26] Yu H, Jian Y, Charalampos B, Xinger W, Xiaowei D. Dynamic analysis of offshore steel wind turbine towers subjected to wind, wave and current loading during construction. Ocean Eng 2020;216:108084. http://dx.doi.org/10.1016/j.oceaneng.2020.108084.
[27] Quilligan A, O'Connor A, Pakrashi V. Fragility analysis of steel and concrete wind turbine towers. Eng Struct 2012;36:270–82. http://dx.doi.org/10.1016/j.engstruct.2011.12.013.
[28] Wang J, Qin D, Lim TC. Dynamic analysis of horizontal axis wind turbine by thin-walled beam theory. J Sound Vib 2010;329(17):3565–86. http://dx.doi.org/10.1016/j.jsv.2010.03.011.
[29] Harte M, Basu B, Nielsen S. Dynamic analysis of wind turbines including soil-structure interaction. Eng Struct 2012;45:509–18. http://dx.doi.org/10.1016/j.engstruct.2012.06.041.
[30] Hernandez-Estrada E, Lastres-Danguillecourt O, Robles-Ocampo JB, Lopez-Lopez A, Sevilla-Camacho PY, Perez-Sariñana BY, Dorrego-Portela JR. Considerations for the structural analysis and design of wind turbine towers: A review. Renew Sustain Energy Rev 2021;137:110447. http://dx.doi.org/10.1016/j.rser.2020.110447.
[31] Basu B. Tower design and analysis. In: Tong W, editor. Wind power generation and wind turbine design. WIT transactions on state-of-the-art in science and engineering, vol. 44, WIT Press; 2010, p. 527–57. http://dx.doi.org/10.2495/978-1-84564-205-1/16.
[32] Ma Y, Martinez-Vazquez P, Baniotopoulos C. Wind turbine tower collapse cases: A historical overview. Proc Inst Civ Eng - Struct Build 2019;172(8):547–55. http://dx.doi.org/10.1680/jstbu.17.00167.
[33] Gesualdo A, Iannuzzo A, Penta F, Monaco M. Nonlinear dynamics of a wind turbine tower. Front Mech Eng 2019;14:342–50. http://dx.doi.org/10.1007/s11465-019-0524-3.
[34] Qian X, Gao Z, Zhang Z, Wang T. Geometric nonlinear dynamic response of wind turbines with different power performance. E3S Web Conf 2021;271:01005. http://dx.doi.org/10.1051/e3sconf/202127101005.
[35] Dai L, Xia D, Chen C. Regular and nonlinear dynamics of horizontal Axis wind turbine blades subjected to fluctuating wind loads. Energy Procedia 2017;110:529–36. http://dx.doi.org/10.1016/j.egypro.2017.03.180, 1st International Conference on Energy and Power, ICEP2016, 14-16 December 2016, RMIT University, Melbourne, Australia.
[36] Lee D, Hodges DH, Patil MJ. Multi-flexible-body dynamic analysis of horizontal Axis Wind Turbines. Wind Energy 2002;5(4):281–300. http://dx.doi.org/10.1002/we.66.
[37] Jiang B, Hui Y, Yang Q, Hua X. Nonlinear dynamic analysis of parked large wind turbine blade considering harmonic inertial excitation using continuum mathematical model. Thin-Walled Struct 2022;181:110128. http://dx.doi.org/10.1016/j.tws.2022.110128.
[38] Sapountzakis EJ, Dikaros IC, Kampitsis AE, Koroneou AD. Nonlinear response of wind turbines under wind and seismic excitations with soil–structure interaction. J Comput Nonlinear Dynam 2015;10(4). http://dx.doi.org/10.1115/1.4027697, 041007.
[39] Lenci S, Rega G. Global nonlinear dynamics for engineering design and system safety. Springer International Publishing; 2019, http://dx.doi.org/10.1007/978-3-319-99710-0.
[40] Larsen J, Nielsen S. Non-linear dynamics of wind turbine wings. Int J Non-Linear Mech 2006;41(5):629–43. http://dx.doi.org/10.1016/j.ijnonlinmec.2006.01.003.
[41] Yuan G, Wang Y. Internal, primary and combination resonances of a wind turbine blade with coupled flapwise and edgewise motions. J Sound Vib 2021;514:116439. http://dx.doi.org/10.1016/j.jsv.2021.116439.
[42] Clementi F, Lenci S, Rega G. 1:1 internal resonance in a two D.O.F. complete system: A comprehensive analysis and its possible exploitation for design. Meccanica 2020;55:1309–32. http://dx.doi.org/10.1007/s11012-020-01171-9.
[43] Jonkman J, Butterfield S, Musial W, Scott G. Definition of a 5-MW reference wind turbine for offshore system development. Technical report NREL/TP-500-38060, National Renewable Energy Laboratory; 2009.
[44] Makarios T, Efthymiou E, Baniotopoulos C. On the torsional–translational response of wind turbine structures. Arab J Sci Eng 2016;41:1241–9. http://dx.doi.org/10.1007/s13369-015-1911-7.
[45] Villaggio P. Mathematical Models for Elastic Structures. Cambridge University Press; 1997, http://dx.doi.org/10.1017/CBO9780511529665.
[46] Lenci S, Clementi F, Mazzilli C. Simple formulas for the natural frequencies of non-uniform cables and beams. Int J Mech Sci 2013;77:155–63. http://dx.doi.org/10.1016/j.ijmecsci.2013.09.028.
[47] Nayfeh AH, Mook DT. Nonlinear oscillations. John Wiley & Sons; 1995, http://dx.doi.org/10.1002/9783527617586.
[48] Lenci S. An asymptotic approach for large amplitude motions of generic nonlinear systems. Internat J Engrg Sci 2023;192:103928. http://dx.doi.org/10.1016/j.ijengsci.2023.103928.
[49] Sander A, Meinhardt C, Thoben K-D. Monitoring of offshore wind turbines under wave and wind loading during installation. In: Papadrakakis M, Fragiadakis M, C. P, editors. Proceedings of EURODYN 2020 - XI international conference on structural dynamics. Athens, Greece; 22–24 June 2020, p. 2189–205.